

**Evidence of High Relief Eocene Topography in the Southern Idaho  
Batholith and Constraints on Rift-related Exhumation in the Miocene  
Western Snake River Plain, Idaho, Using Apatite (U-Th)/He  
Thermochronometry**

A Thesis

Presented in Partial Fulfillment of the Requirements for the

Degree of Master of Science

with a

Major in Geology

in the

College of Graduate Studies

University of Idaho

by

Kelsey F. Wetzel

Major Professor: Jessica Stanley, Ph.D.

Committee Members: Elizabeth Cassel, Ph.D.; Renee Love, Ph.D.

Department Administrator: Leslie Baker, Ph.D.

August 2020

### Authorization to Submit Thesis

This thesis of Kelsey F. Wetzel, submitted for the degree of Master of Science with a Major in Geology and titled "Evidence of High Relief Eocene Topography in the Southern Idaho Batholith and Constraints on Rift-related Exhumation in the Miocene Western Snake River Plain, Idaho, Using Apatite (U-Th)/He Thermochronometry," has been reviewed in final form. Permission, as indicated by the signatures and dates below, is now granted to submit final copies to the College of Graduate Studies for approval.

Major Professor: \_\_\_\_\_ Date: \_\_\_\_\_  
Jessica Stanley, Ph.D.

Committee Members: \_\_\_\_\_ Date: \_\_\_\_\_  
Elizabeth Cassel, Ph.D.

\_\_\_\_\_ Date: \_\_\_\_\_  
Renee Love, Ph.D.

Department

Administrator: \_\_\_\_\_ Date: \_\_\_\_\_  
Leslie Baker, Ph.D.

## Abstract

The western Snake River Plain (WSRP) in southwest Idaho has been characterized as an intracontinental rift basin but differs markedly in orientation and style from other western Cordilleran extensional structures. Understanding the rifting history of the WSRP and exhumation of its mountainous flanks can have implications for other intracontinental rift basins and for the topographic evolution of this region within a broader tectonic context. We sampled granitoid bedrock from Cretaceous and Eocene-aged plutons from the flanks of the WSRP to detail their exhumation history with apatite (U-Th)/He (AHe) thermochronometry. We present new AHe dates from seventeen samples, with cooling dates ranging from  $7.9 \pm 1.4$  Ma to  $55 \pm 10$  Ma. The majority of cooling dates for the Cretaceous plutons are Eocene, and the Eocene intrusions yield Miocene dates. The AHe dates provide thermochronological evidence of rapid cooling and exhumation of the Idaho batholith during the Eocene. This supports the presence a high relief landscape in Idaho associated with regional uplift due to Farallon slab rollback and Challis magmatism. This high landscape was rapidly eroded and supplied massive amounts of sediment to Eocene basins across the Cordillera. We also find evidence for a post-Eocene decrease in relief, seen in the negative slope on date-elevation relationships in the southwest flank of the WSRP. Our AHe dates indicate limited exhumation on the flanks of the WSRP during Miocene rift formation. We interpret this to be evidence of extension dominated by magmatic intrusions and intrabasin faults rather than basin-bounding faults. Focused exhumation  $\sim 20$ -7 Ma seen in the Eocene pluton relates to concentrated incision along the Middle Fork Boise River in the interior of the Boise Mountains due to relative base level fall or more recent uplift due to plume-associated magmatism.

## Acknowledgments

It is with immense gratitude that I acknowledge the support of my supervisor, Dr. Jessica Stanley. Her patient guidance and encouragement made it possible for me to succeed in my graduate studies and navigate the sometimes-rough waters of my thesis research. I am privileged to be Jess's first graduate student and to work with her in my two years at the University of Idaho. I would like to thank my supervisory committee: Dr. Liz Cassel and Dr. Renee Love, for reviewing my thesis, providing valuable comments, and being all-around exceptional professors. I also thank Shannon Conner for being the most excellent field assistant, Dominik Schneider for helping to haul many pounds of rock samples, and Dr. Spencer Wood, who helped initiate me into the mysteries of field work in the WSRP. I appreciate the help of Dr. Paul O'Sullivan and Jim McMillan of GeoSep Services, who kindly hosted me at GeoSeps for two marathon mineral separation campaigns. I would also like to thank GSA for awarding me a Graduate Student Research Grant to help fund my research. Finally, I would like to say thank you to all my fellow graduate students at UI and WSU for scientific discussions, bad science movie nights, and helping make grad school life bearable.

### **Dedication**

I would like to give heartfelt thanks to my family, especially my twin sister, Kazia, and my mom and dad. Their loving support gives me strength.

## Table of Contents

Authorization to Submit Thesis .....	ii
Abstract .....	iii
Acknowledgments.....	iv
Dedication .....	v
Table of Contents .....	vi
List of Tables .....	vii
List of Figures .....	viii
Introduction.....	1
Geologic Setting.....	4
Tectonic Evolution of the Western U.S. ....	4
Topographic Evolution of the Northern Rocky Mountains .....	5
Geology and Study Area .....	6
Previous Thermochronology.....	8
(U-Th)/He Thermochronology Background .....	8
Sampling Strategy, Methods, and Results .....	12
Sampling Strategy .....	12
(U-Th)/He Methods.....	13
Thermal History Modeling Methods.....	14
Results .....	17
Discussion .....	19
Paleogene Exhumation and Topography .....	19
Miocene Extension.....	26
Miocene Landscape Rejuvenation and Incision.....	29
Conclusions .....	33
References .....	35

**List of Tables**

Table 1.1 Apatite (U-Th)/He data from southwest Idaho.....	15
Table 1.2 Thermal history model input for southwest Idaho samples.....	18

## List of Figures

Figure 1.1 Map showing southern Idaho topography, regional structures, and locations of samples in this study of previously published thermochronology samples .....	9
Figure 1.2 Geologic map showing sample transect locations in this study .....	11
Figure 1.3 AHe date-eU plots and thermal history modeling results for Owyhee samples.....	22
Figure 1.4 AHe date-eU plots and thermal history modeling results for Boise samples.....	23
Figure 1.5 Date-elevation profiles for all transects.....	24
Figure 1.6 Schematic crustal cross sections across the WSRP for the Eocene - Present.....	30

## Introduction

Reconstructing paleotopography is fundamental to our understanding of erosional and exhumational processes, mantle dynamics, lithospheric deformation, weather and climate, and feedbacks between these systems. Understanding the mechanisms influencing regional topographic change within the Cordillera is still a field of active study (e.g., Cassel et al., 2014, 2018; Heller et al., 2016; Stevens et al., 2017; Schwartz et al., 2019; Becker et al., 2014; Zhou & Liu, 2019). The North American Cordillera has large topographic variability that has been influenced by diverse tectonic events and surface and mantle processes. Even considering the large variability, Idaho topography is noticeably unique and distinct (Fig. 1.1). Thus, addressing the evolution of topography Idaho and the driving mechanisms of extension in the western Snake River Plain (WSRP) will provide valuable insights into earth processes in this region and the western US.

The geologic history of western Idaho is distinct even within the northern Rocky Mountains region. The Idaho batholith, one of a string of large batholiths along the margin of the Cordillera, was emplaced entirely into Precambrian continental crust, adjacent to the major near-vertical lithospheric boundary between island-arc accreted terranes to the west and the North American craton (e.g., Gaschnig et al., 2010). Geochemical analyses of the Atlanta peraluminous suite, which forms most of the Atlanta lobe of the batholith, indicates it was largely the result of crustal melting, unlike other batholiths that were emplaced into oceanic accreted terranes (e.g., Gaschnig et al., 2011; Byerly et al., 2016). The western Snake River Plain (WSRP) borders the southern Idaho batholith and separates the bulk of the batholith from the associated Silver City pluton. Though a structurally controlled rift, the WSRP has very different topographic characteristics from the tilted block (“domino-style”) Basin and Range rifts and metamorphic core complexes that dominate extensional basins in the Cordillera (e.g., Wood & Clemens, 2002). It lacks major long faults that have evidence of significant throw (vertical offset), and the rift is significantly wider than most grabens in the Basin and Range Province (e.g., Malde, 1991; Eaton, 1982). Despite the unique characteristics of the Idaho batholith and WSRP, they have been far less extensively studied than other Cordilleran batholiths and rifts (e.g., Saleeby et al., 2008; Lackey et al., 2008; Hildebrand & Whalen, 2014; Alsleben et al., 2012; Byerly & Lassiter, 2012; Ricketts et al.,

2008), but can potentially provide insights into the tectonic, surface, and deep-seated processes at work in western North America.

Continental rifting is an important part of the tectonic cycle, but the processes governing rift initiation, fault geometries, location of extension, and extension mechanisms remain an active area of study (Nelson et al., 1992; Peace et al., 2019; Min & Hou, 2019). Simply put, continental rifting is caused by the interactions between mantle flow and plate movements. However, many crustal, lithospheric, and mantle factors combine to influence the structure, mechanisms, and rates of rifting, so numerous expressions of rifting exist – wide or narrow, large basin-bounding faults or numerous intrabasin faults or en echelon geometries, or magma dominated (Abbey & Niemi, 2019, and references therein). The duration of the rifting stage of is also highly variable, and stress field changes can cause abrupt termination of rifting (Ziegler & Cloetingh, 2004). A better understanding of the mechanisms and style of WSRP rifting can provide insight into why it differs so much from other extensional structures in the western US and what that implies about continental rifting processes and extension in the western US.

Various driving mechanisms for extension have been proposed for the WSRP that have different implications for the evolution of the structure. Three main models have been proposed which predict different spatio-temporal patterns of faulting and flank exhumation. The first model is extension driven by lithospheric stresses caused by the eruption of the Columbia River Basalt Group (CRBG), a continental flood basalt province that covers parts of Oregon, Washington, and Idaho (Fig. 1.1; Camp & Ross, 2004; Glen & Ponce, 2002; Shervais et al., 2002). This suggests that the trend of the WSRP fits into a radial pattern of extensional structures including the Oregon Idaho graben, the northern Nevada rifts, and several CRBG-related dike swarms and that the pattern is due to a point stress at the base of the lithosphere from the upwelling source of CRBG volcanism (Glen & Ponce, 2002). This model implies the upwelling source's point-like stress on the lithosphere was strong enough to induce continental rifting and may predict a NW to SE pattern of extension initiation and flank exhumation contemporaneous with peak CRBG activity ca. 16 Ma. A second model is that WSRP extension is driven by the Yellowstone plume since many workers suggest the Yellowstone hotspot represents a mantle plume tail being overridden by continental

lithosphere (e.g., Morgan, 1972; Pierce & Morgan, 1992; Shervais & Hanan, 2008; Smith & Braile, 1994). In this model, WSRP extension is driven by thermal tumescence due to focused upwelling of the mantle plume tail when it was located at the Bruneau-Jarbidge eruption center (with peak activity from 12-10 Ma; Bonnicksen et al., 2008) at the southeast end of the WSRP (Beranek et al., 2006; Clemens, 1993; Wood & Clemens, 2002; Shervais et al., 2002). In this model, the Yellowstone hotspot initiated continental extension and had significant topographic uplift associated with it (e.g., Beranek et al., 2006; Pierce & Morgan, 1992, 2009). The Yellowstone model predicts that initiation and most rapid exhumation on WSRP normal faults occurred during Bruneau-Jarbidge eruptive center activity and implies a SE to NW pattern of faulting and possibly more significant fault offset and footwall exhumation on the SE end of the structure close to Bruneau-Jarbidge. The third model is that extension is not correlated with CRBG or Yellowstone hotspot activity, but that the WSRP may represent slightly atypical Basin and Range extension as implied by similar horizontal stress orientations for fractures and faults at depth within the WSRP to Basin and Range structures in northern Nevada (Kessler et al., 2017). In this case, fault initiation and flank exhumation might be expected to be uniform along the fault length or maximal in the center of the fault (e.g., Ellis & Barnes, 2015; Densmore et al., 2004) rather than related to magmatic centers. Other potential drivers may contribute to exhumation, though not WSRP extension. These drivers include erosional exhumation driven by Miocene climate variations (Sun & Zhang, 2008), or changes in base level due to large fluctuations of paleo Lake Idaho (Swirydczuk et al., 1979). In these scenarios, we might expect to see focused cooling ages during the mid-Miocene Climatic Optimum (~17-15 Ma; Zachos et al., 2008) or during the life cycle of Miocene-Pliocene Lake Idaho (e.g., Wood & Clemens, 2002).

Exhumation patterns can differentiate between these models for WSRP formation, and this study presents new apatite (U-Th)/He (AHe) thermochronologic data from the mountainous flanks of the WSRP to document the timing and patterns of exhumational cooling. Exhumation patterns are interpreted within the framework of broader-scale tectonic processes to help identify mechanisms driving extension in the WSRP rift and how it fits within the erosional and topographic history of the region.

## Geologic Setting

### Tectonic Evolution of the Western U.S.

The tectonic history of the North American Cordillera since the Jurassic has been dynamic and diverse. Eastward subduction of the Farallon plate under the North American plate is associated with terrane accretion, crustal shortening and thickening, and high regional elevations (e.g., Sevier thrust belt, Dickinson, 2004; Yonkee & Weil, 2015). Additionally, long lived subduction produced a series of large igneous batholiths along the continental margin between ~125-60 Ma, including the Coast Mountains, Sierra Nevada, Peninsular Range, and Idaho batholiths (e.g., DeCelles et al., 2009; Gehrels et al., 2009; Ducea, 2001; Premo et al., 2014; Gaschnig et al., 2010). A change in the subduction angle of the Farallon plate to flat or subhorizontal in the Late Cretaceous contributed to the deep-seated Laramide orogeny, a deformation belt ~700-1500 km inboard of the convergent margin, and the eventual shut off of Cordilleran arc magmatism (DeCelles et al., 2009; English & Johnston, 2004), though the mechanism of flat slab subduction has not been precisely defined (e.g., Liu & Currie, 2015). Post-Laramide slab delamination and resulting asthenospheric upwelling ca. 55-24 Ma produced sweeping large-volume magmatism, regional uplift, extension, and sedimentation across the western United States, as well as led to the establishment of the Cascadia subduction zone (e.g., Cassel et al., 2018; Humphreys, 1995).

In the early Miocene, Basin and Range regional extension of the overthickened crust was triggered by the change in the western North American plate boundary and relative plate motion at the end of Farallon slab subduction (e.g., Dickinson, 2004; Yonkee & Weil, 2015). Extension was accompanied by a surge in volcanism in the Miocene, including the voluminous Columbia River Basalt Group (CRBG) in Oregon, Idaho, and Washington, which erupted 95% of its volume between 16.7 and 15.9 Ma (Kasbohm & Schoene, 2018). The mechanism behind CRBG volcanism has been widely debated, with some workers attributing its formation to mantle plume head impingement (e.g., Camp, 1995; Geist & Richards, 1993), back arc processes such as tearing (Liu & Stegman, 2012) or Farallon slab rollback (Long et al., 2012), or lithospheric foundering (Hales et al., 2005). Since ~16 Ma, mantle plume impingement on the base of the North American lithosphere from the Yellowstone plume has produced a northeast-trending path of volcanic fields from northwest

Nevada across southern Idaho to Wyoming that tracks with North American plate movement (Pierce & Morgan, 1992).

### **Topographic Evolution of the Northern Rocky Mountains**

The tectonic history of the western U.S. is consistent with the existence of high paleo-elevations in the northern Rocky Mountains region through Late Cretaceous and Paleogene time. Fayon et al. (2017) posit that the emplacement and cooling history of the southern Idaho batholith is explained by a Late Cretaceous-Paleogene plateau in Idaho – the northern extent of the high elevation thrust belt-thickened hinterland sometimes termed the Nevadaplano (e.g., Axelrod, 1997; Best et al., 2016; DeCelles, 2004; Cassel et al., 2014, 2018). The lack of consistently oriented fabrics within the Atlanta lobe of the batholith, which was emplaced during Sevier orogenic regional contraction, suggests it was intruded into a neutral or extensional tectonic setting like a crustal plateau (Byerly et al., 2016). Additional evidence of high paleo-topography during this time is that the signature 2-mica granite of the Idaho batholith is a major sediment source for a variety of Paleogene basins across the Cordillera, including the Franciscan Basin in California (e.g., Dumitru et al., 2013), the Green River Basin in Wyoming (e.g., Chetel et al., 2011), and the Tyee forearc in coastal Oregon (e.g., Heller et al., 1985). Paleoelevation studies imply Paleogene elevations in the Cordillera were likely higher than today (Wolfe et al., 1998; Kent-Corson et al., 2006). In concert with the high regional elevations was a migratory extensional and volcanic arc that swept across the Rocky Mountain region associated with Farallon slab rollback, showing a progressive younging pattern to the west and south from ~60-27 Ma (e.g., Dickinson, 2004). In the northern Rocky Mountains this sweep included the early to middle Eocene Idaho Challis and Wyoming Absaroka volcanics (~52-42 Ma) and the development of metamorphic core complexes in Montana and Idaho (e.g., Bitterroot, Anaconda, Pioneer-Boulder, Beranek et al., 2006; Hiza, 1999; Foster & Raza, 2002; Foster et al., 2010; Vogl et al., 2012).

Miocene to recent topography in the northern U.S. Cordillera has been marked by continued volcanism. In the Pacific Northwest, the Cascadia arc has been a locus of magmatism from the Eocene to the present. In the Cascadia back arc, CRBG lava flows blanketed large portions of Washington, Oregon, and parts of Idaho. Since ~12 Ma, the wake of the Yellowstone volcanic fields formed the topographically down warped eastern Snake

River Plain (ESRP) in Idaho, flanked by the elevated arms of the Yellowstone crescent of high terrain (e.g., Pierce & Morgan, 1992; Vogl et al., 2014). Detrital zircon provenance studies showing the eastward migration of the Snake River drainage suggest a gradual increase in the Snake River's drainage area as the North American plate moved W-SW over the Yellowstone plume (Pierce & Morgan, 1992; Beranak et al., 2006; Wegmann et al., 2007).

### **Geology and Study Area**

Our study area in southwest Idaho is a southwest-northeast swath across the central portion of the WSRP, from the Owyhee Mountains on the southwest flank of the plain to the Boise Mountains on the northeast flank (Figs. 1, 2). There is >1000 m of relief from the peaks within the study area (>2000 m elevation) to the 800-900 m high valley floor of the WSRP. The bedrock of the mountainous flanks consists primarily of Cretaceous granodiorite and two-mica granite and Eocene Challis plutonic rocks that include granodiorite and quartz monzodiorite lithologies (Lewis et al., 2012). In the Owyhee Mountains, Miocene basalt and rhyolite flows of the Silver City volcanics unconformably overlie parts of the granitoid bedrock (Ekren et al., 1981; Bonnicksen et al., 2008). While it might be expected that granitic basement underlies the extended WSRP, high seismic velocities and a large positive Bouguer gravity anomaly beneath the plain suggest there is little granitic crust there or that it has been heavily intruded by dense material such as basalts (Hill & Pakiser, 1967; Mabey, 1976; Wood & Clemens, 2002). Seismic section across the WSRP shows a central basin high (horst), which is likely composed of basalt to satisfy these geophysical requirements (Arney et al., 1982; Shervais et al., 2002; Wood & Clemens, 2002).

The WSRP basin contains 2-3 km of sediments and volcanics deposited between ~17-3 Ma (Malde, 1959; Malde, 1991; Wood & Clemens, 2002; Beranek et al., 2006). The oldest sediments within the WSRP basin are exposed on its flanks and consist of fluvial/lacustrine deposits of the Miocene Payette Formation (north plain) and Miocene Sucker Creek Formation (south plain), which have similarities and are the same age (Forester & Wood, 2012). The Payette Formation is interlayered with lower CRBG basaltic to andesitic volcanics and Weiser basaltic to rhyolitic volcanics (Reidel et al., 2013). The Payette has regional paleoclimate significance because its deposition was coeval with the global mid-

Miocene climatic optimum (Zachos et al., 2001; Kasbohm & Schoene, 2018), and it is the only economic source of hydrocarbons in Idaho (Love et al., 2020). Deposition of fluvial/lacustrine units of the Idaho group followed the Payette and Sucker Creek formations after a depositional hiatus. The Idaho group consists of the late Miocene Poison Creek and Chalk Hills formations and Pliocene Glens Ferry Formation, which were deposited by the extensive paleo-Lake Idaho and are associated with the rifting and subsidence of the WSRP (Love et al., 2020; Wood & Clemens, 2002).

The WSRP is a structurally controlled graben ~40-60 km wide and ~300 km long and bounded by en echelon normal faults (Malde, 1959; Wood & Clemens, 2002; Shervais et al., 2002). The steeply dipping faults have a maximum throw of ~2.9 km (Malde, 1991), with total extension across the graben estimated at 10% (Wood & Clemens, 2002), and with some amount of right lateral slip on north-south extensional duplexes that cross the plain (Hooper et al., 2007). Some workers have suggested that basin formation may have initiated at the northwest end of the WSRP and progressed to the southeast based on the age progression of the initial rhyolite lavas within the graben (Kimmel, 1982; Smith et al., 1982; Swirydczuk et al., 1979). The ages of the range front faults are unknown but they are estimated to be active by at least ~10 Ma and possibly continued later, based on the age of Mount Bennett rhyolite (located in the central Snake River Plain) that is offset by faulting, and the Pliocene age of Lake Idaho sediments that interbed with Mount Bennett Hills volcanics, indicating uplift of the hills continued into the Pliocene (Clemens, 1993; Shervais et al., 2002). The faults cutting Mount Bennet rhyolite are oriented ~N50°W, parallel to the boundary faults on the northeastern margin of the WSRP, indicative of a northeast-southwest extension direction (Clemens & Wood, 1993). K-Ar dates of offset volcanic units on the flanks of the Owyhee Mountains constrain fault initiation to between ~15 and 10 Ma (Clemens, 1993). Most Quaternary fault traces are confined to older Plio-Pleistocene deposits (Wood & Anderson, 1981; Othberg and Stanford, 1992). Recent GPS measurements of strain rates in the northern Basin and Range Province, together with geologic, volcanic, and earthquake data, reveal that the region of the Snake River Plain and Owyhee-Oregon plateau is experiencing a very low strain rate (near zero), separated from the actively extending adjacent Basin and Range regions by shear (Payne et al., 2012).

## Previous Thermochronology

Previous thermochronology studies in the region have focused on the exhumation of the Idaho batholith using apatite and zircon fission track (AFT, ZFT) and zircon (U-Th)/He (ZHe), techniques sensitive to temperatures from ~60-250°C (Fig. 1.1). Studies show that the batholith resided at shallow crustal levels (<100 °C) for much of Cenozoic time (Sweetkind & Blackwell, 1989; Fayon et al., 2017) but indicate spatial variability in exhumation. On the western margin, rocks associated with the border zone and western Idaho shear zone (WISZ) cooled earlier than the core of the batholith (Fig. 1.1, Fayon et al., 2017), cooling below ~350 °C by 85-70 Ma and to <120 °C by ca. 40 Ma (Giorgis et al., 2008). In the central part of the batholith, ZHe ages from the Atlanta lobe exhibit a pattern of cooling as a function of elevation (Fayon et al., 2017). This was interpreted to suggest that the region was thermally stable prior to Eocene Challis magmatism and that post-magmatic isobaric cooling occurred with little to no unroofing, consistent with the existence of a Late Cretaceous-Paleogene plateau in Idaho (Fayon et al., 2017). Like the western border suite, studies of metamorphic core complexes (MCCs) on the east side of the batholith show cooling patterns that differ from the central batholith. AFT and ZFT dates from the Bitterroot MCC show that it exhumed unevenly, with the western side within 1-2 km of the surface by ~48-45 Ma, but the eastern side not exhumed to below 60 °C until after 30 Ma (Fig. 1.1, Foster & Raza, 2002).

Application of the apatite (U-Th)/He (AHe) technique with lower temperature sensitivities (~30-90°C, Farley et al., 2000; Flowers et al., 2009) has been limited to Challis intrusive rocks mostly east of our study area in the Pioneer-Boulder Mountains (Vogl et al., 2014). The Pioneer MCC, located on the northern arm of the Yellowstone crescent of high terrain, has experienced >2-3 km of exhumation since 11 Ma, which was attributed to hotspot-related uplift and exhumation combined with faulting and surface processes (Fig. 1.1, Vogl et al., 2014).

## (U-Th)/He Thermochronology Background

Low temperature thermochronology – including (U-Th)/He dating – has become a key tool in geoscience investigations documenting the timing and tempo of thermal processes, such as mountain building and landscape evolution and erosion. (U-Th)/He thermochronology exploits the radioactive decay of U, Th, and Sm to <sup>4</sup>He and the

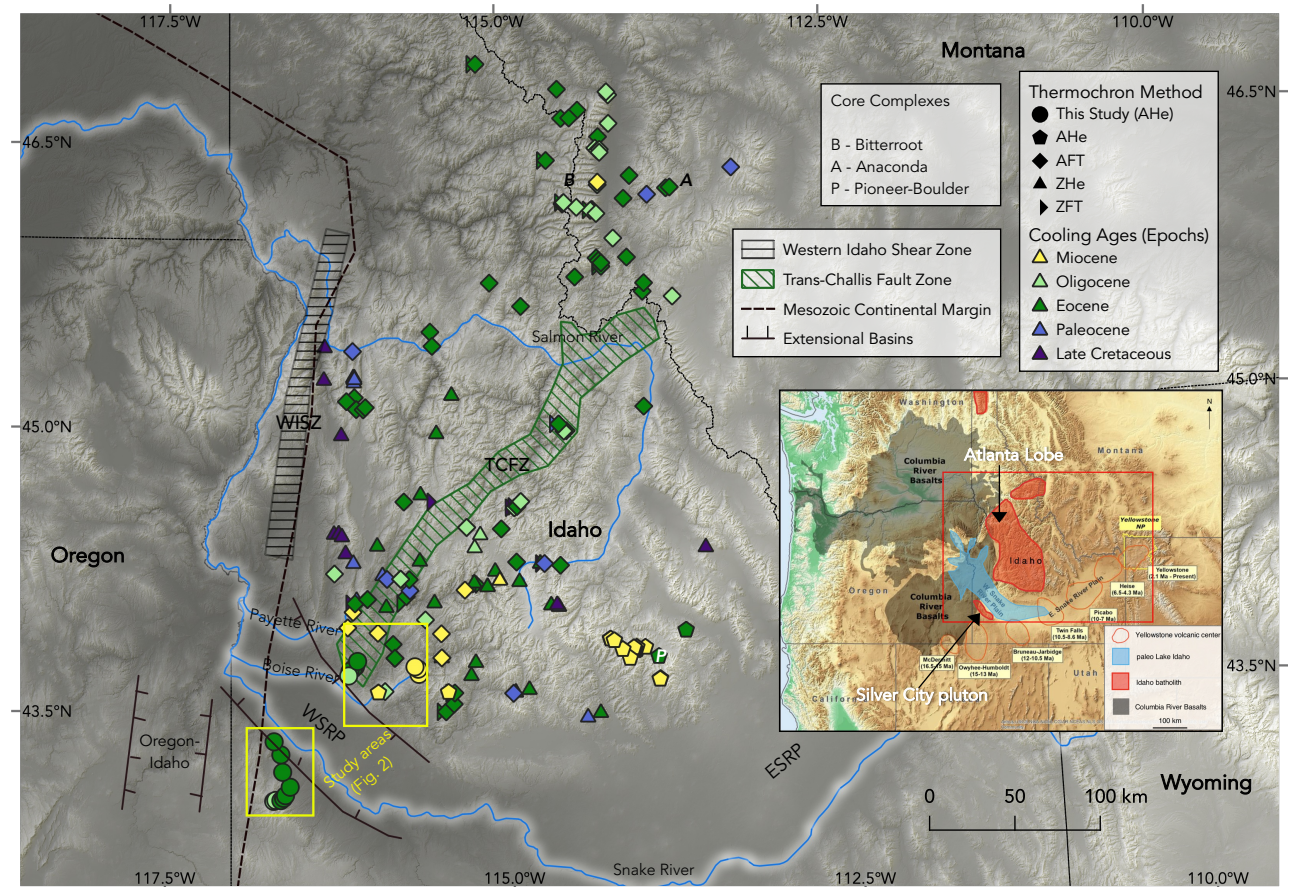


**Figure 1.1.** Terrain map of southern Idaho showing locations and cooling ages of previously published thermochronology samples from Sweetkind & Blackwell (1989), Foster & Raza (2002), Giorgis et al. (2008) and Fayon et al. (2017) and this study. Structural features shown are the paleo continental margin, the surface extent of the western Idaho shear zone (WISZ), the Trans-Challis fault zone, the WSRP and Oregon-Idaho graben, and metamorphic core complexes. Yellow boxes mark the locations of sample transects in Figure 2. Inset figure shows the northwestern US and the extent of the Columbia River Basalts, the Idaho batholith, paleo Lake Idaho, and the track of Yellowstone volcanic centers. The red box outlines the area shown in Fig. 1. Inset figure base map from USGS.gov, modified after Barry et al. (2013), Smith & Siegel (2000), and Christiansen (2001). WSRP – western Snake River Plain; ESRP – eastern Snake River Plain, AFT/ZFT – apatite/zircon fission track, AHe/ZHe – apatite/zircon (U-Th)/He.

temperature-sensitive  $^4\text{He}$  diffusion through the crystal. The He escapes the crystal rapidly at high temperatures and is quantitatively retained at low temperatures. There is a zone of temperature transition between rapid diffusion of He and He retention called the He partial retention zone (PRZ). The temperature range of the PRZ depends on the mineral. The mineral apatite has the relatively low temperature sensitivity of  $\sim 30\text{-}90\text{ }^\circ\text{C}$  (Farley, 2000, Flowers et al., 2009), making it particularly useful for exploring upper crustal processes. The PRZ is also dependent on the radiation damage accumulated in the crystal and the grain size (Shuster et al., 2006; Flowers et al., 2009; Reiners & Farley, 2001, Gautheron et al., 2009). In the apatite (U-Th)/He (AHe) system, accumulated radiation damage increases the apatite He retentivity. Dating apatites with a range of temperature sensitivities allows us to better decipher possible time-temperature (tT) paths experienced by a rock (Flowers et al., 2009). For rocks that are at or near surface for long periods, apatites with higher U and Th concentrations accumulate radiation damage more rapidly than those with lower U and Th concentrations. Crystals with higher radiation damage will thus have higher effective closure temperatures. Rocks that reside in the  $30\text{-}90\text{ }^\circ\text{C}$  PRZ for a long time (experiencing slow cooling) can have AHe dates that positively correlate with effective uranium concentrations ( $eU, [U] + 0.235[\text{Th}]$ ), while rocks that cool rapidly through the PRZ yield similar AHe dates regardless of eU (Shuster et al., 2006; Flowers et al., 2007; Flowers et al., 2009). Several other factors besides radiation damage can contribute to scatter of AHe dates within a sample. These can include grain size variability (Reiners & Farley, 2001), fractured and broken grains (Brown et al., 2013), and fluid and mineral inclusions which contribute excess and parentless He (Vermeesch et al., 2007). Like high radiation damage, these effects are most enhanced in samples that experienced slow cooling scenarios and increased residence time in the PRZ. It is important to note that a measured AHe date is the product of the complete tT path of a sample, and not indicative of a particular thermal event.

An approach for constraining the cooling history of rocks examines AHe date-elevation relationships. This technique evaluates the apparent pattern of thermochronometric dates as a function of structural paleodepth or elevation (e.g., Braun, 2002; Reiners and Brandon, 2006; Stockli, 2005). The expected date-elevation relationship in an actively uplifting and eroding area with finite topography would be to observe older dates in rocks that are at high elevations (i.e., near a mountain top) and younger dates at low elevations because the rocks

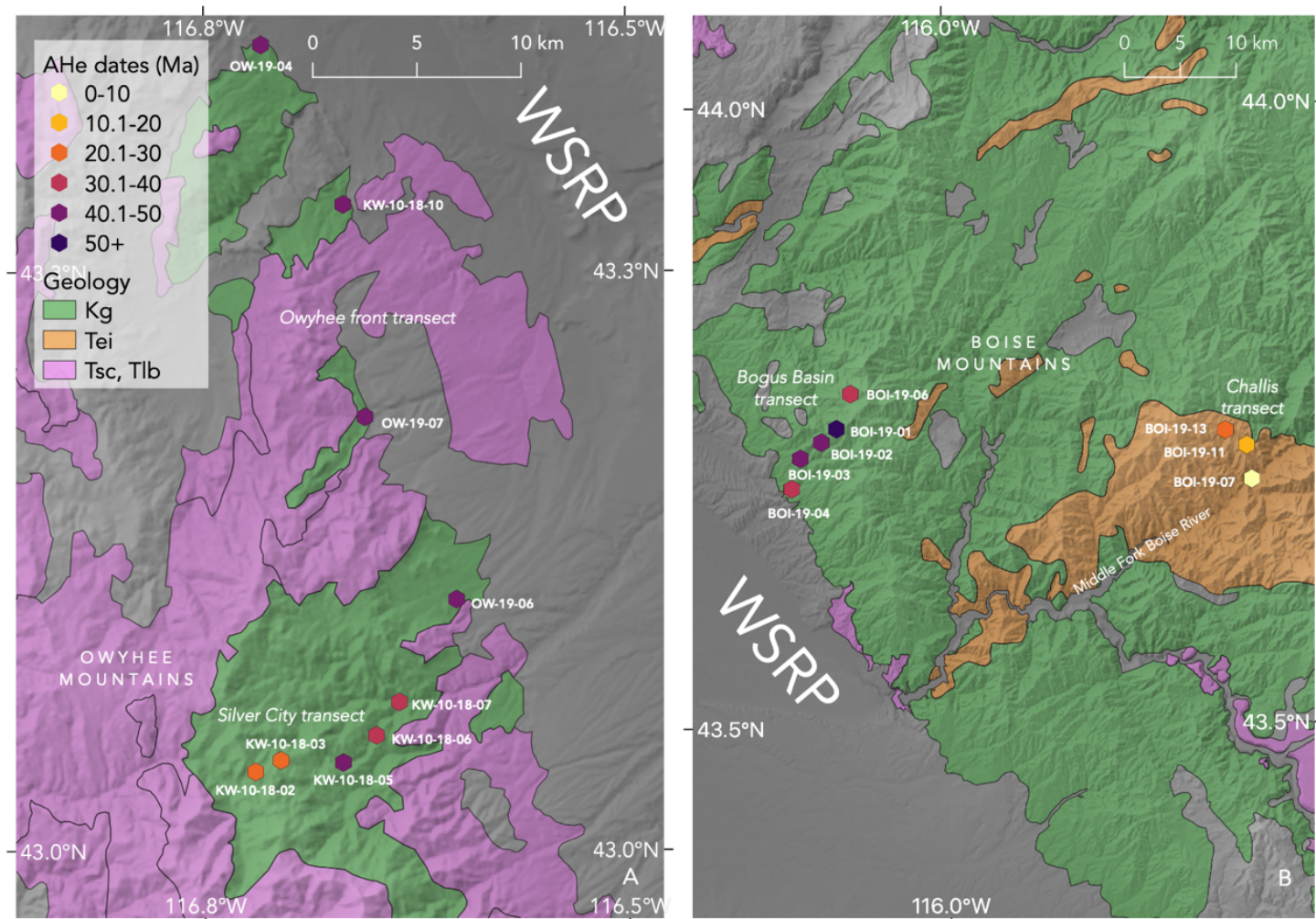


**Figure 1.2.** Geologic map (simplified from Lewis et al., 2012) showing the locations of the Silver City transect and Owyhee front transect in the Owyhee Mountains, southwest flank of the WSRP (A) and the Bogus Basin transect located in the northeast flank of the WSRP and the Challis transect along the Middle Fork Boise River in the Boise Mountains (B). Kg – Cretaceous granitoids, Tei – Eocene Challis intrusive rocks, Tsc – Miocene Silver City Rhyolite, Tlb – Miocene lower basalt.

exhumed near a mountain top have cooled through the closure temperature before rocks that are exhumed near the bottom of a valley (Braun, 2002). The slope of the date-elevation relationship is equal to the exhumation rate in slowly eroding areas, but in rapidly eroding environments the closure temperature isotherm is perturbed by the surface topography and the slope gives an overestimate of the true exhumation rate. The slope of a date-elevation relationship derived from AHe dating is affected strongly by relative surface relief changes. If relief increases, then the slope of the date-elevation relationship decreases to match the real erosion rate more closely. If the amplitude of relief decreases, the slope of the date-elevation relationship is inverted, with the youngest cooling dates observed at high elevations and oldest dates at low elevations (Braun, 2002; House et al. 1998). For rocks collected at the tops of ridges, relief reduction leads to a shortening of the distance the rocks traveled between the time the rocks passed through the PRZ and the time they reached the surface, and conversely, rocks found at valley bottoms will see that distance increased, leading to a reduction in apparent age at ridge tops and increase in apparent age at valley bottoms (Braun, 2002).

In extensional settings, footwall blocks are exhumed by normal fault motion. Prior to faulting, a static crustal block will have an established AHe date pattern with depth that reflects the AHe PRZ (e.g., Stockli, 2005). Then as faulting commences, the crustal block and fossil PRZ are rapidly exposed and cooled through uplift/exhumation of the footwall. Samples collected in a footwall block elevation transect roughly perpendicular to fault strike will allow for evaluation of cooling dates as a function of paleodepth and will display a positive date-elevation relationship. If fault slip magnitude is great enough to expose the entire fossil PRZ, plotting the AHe dates versus elevation (paleodepth) allows for identification of an inflection point in the data trend that marks the base of the fossil PRZ and determines onset of rapid exhumation (e.g., Stockli et al., 2000; Stockli, 2005; Curry et al., 2016).

## **Sampling Strategy, Methods, and Results**

### **Sampling Strategy**

Our sampling strategy was to collect minimally weathered granitic bedrock in three ~1-km elevation transects in the mountainous flanks of the WSRP. Our goal was to effectively

sample the two primary plutons of the Idaho batholith on the northeast and southwest flanks of the WSRP to identify any age-elevation relationships and to reconstruct thermal histories and regional exhumation patterns with the (U-Th)/He method. We collected 23 samples of Cretaceous two-mica granodiorite of the Idaho batholith (Kg) and Eocene granite of the Challis intrusive rocks (Tei), approximately 4-5 kg at each sample location. In the Owyhee Mountains, we sampled one north-south oriented elevation transect (Kg), from the mountain range front (1151 m) to the upper contact between the granite and Miocene volcanic rocks above Silver City, ID (2093 m, the Silver City transect), as well as samples along ~30 km of the range front to identify spatiotemporal changes in exhumation age along the edge of the WSRP (Owyhee front transect). In the Boise Mountains, we sampled one north-south elevation transect from near the range front (1038 m) up to Bogus Basin resort (2018 m) (Kg, the Bogus Basin transect), and an east-west elevation transect from the Middle Fork Boise (MFB) River above Arrowrock Reservoir (1058 m) up the Haga Creek Trail to Bald Mountain (1729 m) (Tei, the Challis transect). Unfortunately, not every sample yielded suitable apatite crystals for dating, but in total we acquired AHe data for seventeen samples across the three elevation transects and Owyhee range front transect (Fig. 1.2; Table 1.1).

Additional field activities included reconnaissance field mapping in the Owyhee Mountains. We used open-source mobile GIS software to ground-check map contacts on the existing geologic map (Ekren et al., 1981) of the Cretaceous granite with overlying volcanic units. Contacts were added or altered on the mobile GIS map in the field as needed.

### **(U-Th)/He Methods**

Apatite crystals were separated using standard density and magnetic separation techniques. Apatite crystals were selected individually for (U-Th)/He dating based on crystal form and size and lack of inclusions under cross-polarized light. Each grain was photographed, and its dimensions measured before loading into Nb packets for analysis. Helium measurements were made on an ASI Alphachron™ in the University of Colorado Boulder (CU) Thermochronology Research and Instrumentation Laboratory (CU TRaIL), Boulder, Colorado, USA. Degassed grains were then dissolved and measured for U, Th, and Sm on an Agilent 7900 Quadrupole inductively coupled plasma-mass spectrometer (ICP-MS) at CU TRaIL. After the U, Th, and Sm contents were measured, He dates and all associated

data were calculated on a custom spreadsheet using the methods described in Ketcham et al. (2011). Every batch of samples included standards run sporadically throughout the process to monitor procedures and maintain consistency from run to run.

All data are reported in Table 1. Grains with  $\alpha$ -ejection ( $F_T$ ) corrections of less than 0.56 were excluded as they are considered less reliable. Six grains that are age outliers from the main population are included in Table 1 in italics. These are not included in sample averages or interpretations. Average (U-Th)/He dates and the associated  $1\sigma$  standard deviations are reported for samples with <20% dispersion.

### **Thermal History Modeling Methods**

We used the HeFTy thermal modeling software (Ketcham, 2005) to further evaluate the cooling histories of these rocks. The goal of thermal history modeling is to evaluate what types of thermal histories can satisfy both the AHe data and the geologic observations. HeFTy inverse modeling predicts AHe dates from simulated random time-temperature (tT) paths that conform to geologic constraints input by the user and compares these predicted dates with the measured dates. The inverse modeling reports the paths where the predicted AHe are statistically “acceptable” and “good” fits to the measured data (see Table 2 and Ketcham, 2005 for statistical measures). The geologic constraints are boxes drawn in HeFTy that define regions in tT space through which the thermal history must pass. The detailed data and constraints used for each model are summarized in Table 2. The geologic constraints for all samples from the Boise Mountains included high temperatures at the time of pluton emplacement in the crust (temperatures  $>120$  °C) at  $\sim 90$ -65 Ma for Kg rocks and  $\sim 52$ -42 Ma for Tei rocks (Gaschnig et al., 2010) and an average surface temperature of  $10 \pm 5$  °C at present. Actual magmatic temperatures are not needed for modeling pluton emplacement because the AHe system is not sensitive to temperatures above  $\sim 120$  °C, and therefore HeFTy cannot constrain tT paths of AHe data at high temperatures. In the Owyhee Mountains, there is abundant field evidence that granitoid rocks were exposed at the surface by the mid-Miocene ( $\sim 16$ -15 Ma), when basalt and rhyolite units were deposited on the granite (Bonnichsen et al., 2008; Pansze, 1975). Thus, Owyhee sample models include constraint boxes for Kg emplacement age, then allow for the surface to be reached between 21-16 Ma and for possible reheating by contact with volcanic flows and/or burial between 16-10 Ma,

TABLE 1. Apatite (U-Th)/He Data from Southwest Idaho

Sample <sup>a</sup>	Mass ( $\mu\text{g}$ )	$r^b$ ( $\mu\text{m}$ )	Term <sup>c</sup>	He (ncc)	U (ppm)	Th (ppm)	Sm (ppm)	eU <sup>d</sup> (ppm)	Th/U	Raw Date (Ma)	$F_T^e$	Cor. Date (Ma)	$2\sigma^f$ (Ma)
<b>Owyhee Mountains (SW flank of WSRP)</b>													
<b>KW-10-18-02:</b> Cretaceous 2-mica granite of the Idaho batholith (Kg): 43.0343°N, 116.72016°W, 2093 m elev.													
a1	1.12	34.2	0T	0.01	3.84	1.46	14.9	4.20	0.38	14.9	0.60	24.3	3.7
a2	1.16	37.4	1T	0.02	4.31	4.69	17.5	5.40	1.09	24.1	0.63	38.0	5.2
a3	1.35	40.8	2T	0.04	15.5	5.90	31.8	16.9	0.38	14.9	0.66	22.5	1.2
a4	1.08	37.1	2T	0.06	14.3	16.7	31.9	18.2	1.17	23.8	0.62	38.2	3.2
a5	3.12	49.7	0T	0.06	11.5	1.15	19.0	11.7	0.10	14.7	0.73	20.2	1.3
a6	1.23	37.9	2T	0.04	15.6	4.11	28.2	16.5	0.26	14.4	0.63	22.6	2.7
a8	2.13	47.2	1T	0.05	14.3	1.42	28.1	14.6	0.10	13.9	0.71	19.5	1.7
30% standard deviation of AHe dates													
Published mean Kg age: $75 \pm 2$ Ma, zircon U-Pb (Atlanta peraluminous suite) (Gaschnig et al., 2010), applies to all Kg in this study													
<b>KW-10-18-03:</b> Kg: 43.03918°N, 116.70517°W, 1886 m elev.													
a1	2.95	52.5	1T	0.02	4.22	1.13	14.4	4.50	0.27	14.7	0.74	19.8	1.4
a2	0.86	32.4	1T	0.07	32.0	1.74	22.4	32.4	0.05	19.5	0.58	33.3	1.5
a4	11.0	81.0	1T	0.27	7.76	0.77	17.5	7.90	0.10	25.4	0.83	30.5	1.3
a5	6.49	69.1	2T	0.37	10.7	3.90	24.3	11.6	0.37	39.5	0.80	49.4	4.7
a6	3.05	50.3	0T	0.03	4.81	0.18	14.7	4.8	0.04	17.8	0.73	24.2	2.6
a7	4.13	59.0	1T	0.18	16.1	1.47	26.6	16.5	0.09	21.0	0.77	27.3	0.9
a8	1.02	36.4	1T	0.02	9.65	4.38	22.4	10.7	0.45	14.9	0.63	23.6	3.9
Mean: $26.5 \pm 4.9$ Ma, 18% standard deviation													
<b>KW-10-18-05:</b> Kg: 43.03817°N, 116.66843°W, 1474 m elev.													
a2	1.68	41.6	0T	0.84	15.1	1.36	18.9	15.4	0.09	26.7	0.68	39.2	4.2
a3	1.90	47.8	2T	0.06	7.60	0.99	32.7	7.80	0.13	33.4	0.71	46.5	3.6
a4	1.00	37.9	2T	0.02	5.23	0.59	30.4	5.40	0.11	35.4	0.64	54.2	2.2
a5	1.58	44.7	2T	0.13	18.8	0.86	29.1	19.0	0.05	33.9	0.69	48.5	5.2
Mean: $47.1 \pm 6.1$ Ma, 13% standard deviation													
<b>KW-10-18-06:</b> Kg: 43.04988°N, 116.64882°W, 1271 m elev.													
a1	1.09	35.8	0T	0.05	19.2	3.64	16.7	20.0	0.19	18.7	0.63	29.9	4.6
a2	1.92	46.6	2T	0.37	15.6	8.24	31.2	17.5	0.53	88.7	0.70	126	19
a3	4.69	61.9	1T	0.33	13.1	0.54	22.6	13.2	0.04	43.4	0.78	55.5	3.0
a5	4.67	59.4	1T	0.15	12.6	1.36	23.2	12.9	0.11	20.1	0.77	26.1	1.8
43% standard deviation of AHe dates													
<b>KW-10-18-07:</b> Kg: 43.06426°N, 116.63524°W, 1151 m elev.													
a1	1.88	36.5	0T	0.06	10.6	8.09	20.2	12.5	0.76	20.8	0.62	33.6	2.1
a2	4.05	53.2	1T	0.15	9.24	9.39	33.1	11.4	1.02	26.4	0.73	35.8	1.7
a3	0.73	31.0	0T	0.03	13.7	13.0	23.2	16.7	0.95	21.2	0.56	37.4	3.3
a4	0.98	37.9	2T	0.08	12.6	18.6	56.5	17.0	1.47	40.1	0.63	63.0	5.3
a5	3.80	57.0	1T	0.18	11.7	10.6	12.7	14.2	0.91	26.9	0.75	35.7	1.3
a6	0.68	33.0	2T	0.03	12.8	16.4	47.8	16.6	1.29	21.5	0.57	37.0	4.8
Mean: $35.9 \pm 1.5$ Ma, 4% standard deviation													
<b>KW-10-18-10:</b> Kg: 43.27931°N, 116.66751°W, 976 m elev.													
a1	0.83	33.5	1T	0.13	33.3	41.5	23.5	43.0	1.25	28.8	0.59	49.0	1.8
a2	4.45	55.8	1T	0.83	31.7	43.1	20.4	41.8	1.36	36.6	0.74	49.2	2.7
a3	2.77	48.1	1T	0.47	28.1	39.0	17.6	37.2	1.39	37.3	0.70	52.9	1.9
a4	1.72	42.6	2T	0.32	32.2	75.6	51.1	49.9	2.35	30.6	0.66	46.4	1.9
a5	1.81	44.0	2T	0.30	32.8	33.7	19.8	40.7	1.03	33.0	0.68	48.5	1.6
a6	3.13	52.3	2T	0.66	39.4	43.5	17.1	49.6	1.10	34.7	0.73	47.7	3.2
Mean: $49.3 \pm 2.7$ Ma, 5% standard deviation													
<b>OW-19-04:</b> Kg: 43.3484°N, 116.71583°W, 861 m elev.													
a1	3.26	56.3	2T	0.67	31.2	45.1	19.6	41.7	1.45	40.2	0.74	54.0	2.9
a2	3.96	52.5	1T	0.68	30.4	37.0	11.5	39.1	1.22	35.9	0.73	49.2	1.7
a3	2.52	45.9	2T	0.22	19.3	27.7	11.5	25.8	1.43	27.1	0.69	39.4	2.7
a4	3.40	50.6	1T	0.25	15.6	18.0	7.65	19.9	1.15	30.7	0.72	42.7	2.7
a5	1.99	41.5	1T	0.10	11.7	15.1	7.03	15.3	1.29	27.9	0.66	42.4	2.2
a6	2.50	45.3	1T	0.24	12.3	17.4	9.91	16.3	1.43	48.4	0.68	70.5	3.0
Mean: Date-eU trend. $45.5 \pm 5.9$ Ma, 13% standard deviation													
<b>OW-19-06:</b> Kg: 43.10856°N, 116.6012°W, 1186 m elev.													
a1	8.48	73.2	2T	0.25	5.51	7.88	23.1	7.4	1.43	31.5	0.80	39.1	2.4
a2	4.53	56.1	0T	0.05	1.38	2.38	11.7	1.90	1.72	42.2	0.74	56.0	7.1
a3	2.29	48.8	2T	0.12	5.17	7.34	27.0	6.90	1.42	61.6	0.71	86.4	13
a4	1.35	39.2	1T	0.22	36.8	5.45	27.7	38.1	0.15	34.6	0.65	52.7	3.1
a5	7.40	71.5	1T	0.27	2.70	5.64	22.5	4.00	2.09	71.2	0.80	88.5	5.6
Mean: $49.3 \pm 8.9$ Ma, 18% standard deviation													

Table 1. Apatite (U-Th)/He Data from Southwest Idaho (*continued*)

Sample <sup>a</sup>	Mass ( $\mu\text{g}$ )	<sup>b</sup> ( $\mu\text{m}$ )	Term <sup>c</sup>	He (ncc)	U (ppm)	Th (ppm)	Sm (ppm)	eU <sup>d</sup> (ppm)	Th/U	Raw Date (Ma)	F <sub>r</sub> <sup>e</sup>	Cor. Date (Ma)	2 $\sigma$ <sup>f</sup> (Ma)
<b>Owyhee Mountains (<i>continued</i>)</b>													
<b>OW-19-07:</b> Kg: 43.18747°N, 116.65489°W, 1140 m elev.													
a1	1.72	41.9	2T	0.26	40.8	4.74	34.7	41.9	0.12	29.9	0.67	44.4	2.4
a2	1.44	42.4	2T	0.40	76.7	12.4	58.8	79.6	0.16	28.7	0.68	42.4	2.4
a3	1.20	36.6	2T	0.16	44.3	5.29	29.2	45.5	0.12	23.5	0.62	37.5	2.1
a4	1.68	39.2	0T	0.18	29.9	6.49	29.3	31.4	0.22	28.6	0.65	43.8	1.8
a5	1.37	39.9	2T	0.25	51.1	4.97	36.6	52.3	0.10	28.9	0.65	44.1	3.7
Mean: 42.4 $\pm$ 2.9 Ma, 7% standard deviation													
<b>Boise Mountains (NE flank of WSRP)</b>													
<b>BOI-19-01:</b> Kg: 43.74104°N, 116.12158°W, 1819 m elev.													
a1	4.76	56.6	1T	0.97	46.4	1.51	27.0	46.8	0.03	35.6	0.76	47.0	2.5
a2	2.00	44.35	1T	0.59	73.7	4.12	28.9	74.6	0.06	32.7	0.69	47.1	3.7
a3	2.01	44.36	1T	0.46	43.0	1.91	24.6	43.4	0.04	43.3	0.69	62.3	4.4
a4	1.32	36.2	1T	0.25	48.1	1.85	26.6	48.6	0.04	31.4	0.62	50.2	5.9
a5	1.11	37.7	2T	0.39	64.0	2.80	39.8	64.5	0.04	44.5	0.64	69.5	4.8
Mean: 55.2 $\pm$ 10 Ma, 18% standard deviation													
<b>BOI-19-02:</b> Kg: 43.7303°N, 116.13871°W, 1597 m elev.													
a2	0.77	32.0	1T	0.11	34.6	5.41	37.6	35.9	0.16	31.0	0.58	53.1	5.0
a3	1.33	39.6	2T	0.54	103	17.3	61.8	107	0.17	31.4	0.65	48.1	1.8
a4	2.04	43.7	1T	0.22	25.1	2.73	28.1	25.7	0.11	34.4	0.69	50.0	3.4
a5	2.15	44.9	1T	0.28	32.7	4.19	41.9	33.7	0.13	31.4	0.69	45.0	3.2
a6	10.1	76.8	1T	0.69	16.0	2.14	24.1	16.5	0.13	33.9	0.82	41.3	2.4
Mean: 47.5 $\pm$ 4.5 Ma, 10% standard deviation													
<b>BOI-19-03:</b> Kg: 43.71744°N, 116.16193°W, 1412 m elev.													
a1	1.68	44.5	2T	0.16	20.1	3.41	46.1	20.9	0.17	37.1	0.69	53.4	3.0
a3	3.56	54.0	1T	0.22	16.4	12.3	45.5	19.3	0.75	26.1	0.74	35.1	2.3
a4	6.64	68.5	1T	0.58	16.7	2.70	26.6	17.3	0.16	41.3	0.80	51.6	1.1
a5	3.34	48.3	1T	0.29	22.9	3.30	44.7	23.7	0.14	29.6	0.71	41.3	1.7
Mean: 45.3 $\pm$ 8.7 Ma, 19% standard deviation													
<b>BOI-19-04:</b> Kg: 43.69299°N, 116.171871°W, 1038 m elev.													
a1	2.00	45.4	1T	0.25	41.0	3.38	30.9	41.8	0.08	24.6	0.70	35.0	2.2
a3	2.07	45.4	1T	0.19	23.6	22.5	27.6	28.9	0.95	26.6	0.69	38.4	1.5
a4	0.78	30.6	0T	0.05	31.9	2.46	39.8	32.5	0.08	15.4	0.57	27.1	1.3
a5	0.67	31.9	1T	0.06	47.2	2.59	37.2	47.8	0.06	14.2	0.59	24.2	4.6
21% standard deviation of AHe dates													
<b>BOI-19-06:</b> Kg: 43.76918°N, 116.10558°W, 2018 m elev.													
a1	3.48	51.5	1T	0.44	30.9	14.4	27.8	34.3	0.47	29.8	0.73	40.8	0.9
a2	1.77	41.7	2T	0.23	40.2	14.2	30.9	43.6	0.35	24.4	0.67	36.6	1.7
a3	2.49	49.7	2T	0.38	44.1	16.4	32.3	47.9	0.37	26.0	0.72	36.1	1.5
a4	2.99	46.8	1T	0.39	35.7	18.5	29.4	40.0	0.52	26.7	0.70	38.0	1.7
a5	1.72	41.0	1T	0.16	26.5	12.4	25.9	29.4	0.47	26.2	0.66	39.4	3.5
Mean: 38.2 $\pm$ 2.0 Ma, 5% standard deviation													
<b>Boise Mountains (Middle Fork Boise River)</b>													
<b>BOI-19-07:</b> Granite and quartz monzodiorite of Eocene Challis intrusive rocks (Tei): 43.69686°N, 115.66013°W, 1058 m elev.													
a1	0.88	36.6	2T	0.02	32.3	65.1	76.3	47.6	2.02	4.44	0.61	7.26	0.6
a2	0.92	34.7	1T	0.01	8.48	9.42	42.0	10.7	1.11	4.63	0.60	7.61	1.3
a3	0.92	34.1	1T	0.01	7.53	30.3	56.4	14.7	4.02	3.29	0.57	5.63	0.6
a4	1.84	41.9	2T	0.03	13.5	63.9	67.0	28.5	4.74	5.23	0.64	8.10	0.7
a5	1.08	36.1	1T	0.01	8.52	42.8	56.5	18.6	5.02	5.67	0.59	9.45	0.9
a6	2.8	49.1	1T	0.04	10.7	39.6	57.9	20.1	3.69	6.37	0.70	9.04	0.5
Mean: 7.9 $\pm$ 1.4 Ma, 17% standard deviation													
Published mean age for Tei: 47 $\pm$ 2.1 Ma (Gaschnig et al., 2010), applies to all Tei samples in this study													
<b>BOI-19-11:</b> Tei: 43.72419°N, 115.665°W, 1423 m elev.													
a1	1.64	41.8	1T	0.03	10.5	8.55	48.8	12.5	0.82	9.70	0.67	14.3	1.8
a2	1.71	43.4	1T	0.02	7.85	5.53	51.2	9.10	0.71	10.0	0.68	14.4	0.9
a3	4.78	62.5	1T	0.07	5.81	4.30	40.0	6.80	0.74	16.7	0.78	21.4	2.0
a4	3.45	55.7	1T	0.08	9.55	6.88	50.2	11.2	0.72	16.2	0.75	21.5	1.0
a5	1.95	46.8	2T	0.04	9.48	6.55	40.6	11.0	0.69	13.6	0.70	19.2	1.4
23% standard deviation of AHe dates													

Table 1. Apatite (U-Th)/He Data from Southwest Idaho (*continued*)

Sample <sup>a</sup>	Mass ( $\mu$ g)	r <sup>b</sup> ( $\mu$ m)	Term <sup>c</sup>	He (ncc)	U (ppm)	Th (ppm)	Sm (ppm)	eU <sup>d</sup> (ppm)	Th/U	Raw Date (Ma)	F <sub>T</sub> <sup>e</sup>	Cor. Date (Ma)	2 $\sigma$ <sup>f</sup> (Ma)
<b>Boise Mountains (Middle Fork Boise River) (<i>continued</i>)</b>													
<i>BOI-19-13</i> : Tei: 43.73656°N, 115.68853°W, 1728 m elev.													
a1	1.51	41.3	1T	0.12	27.5	74.5	53.0	45.0	2.71	14.7	0.65	22.5	0.9
a2	1.09	38.9	2T	0.06	26.1	64.3	51.0	41.2	2.46	11.6	0.63	18.4	1.1
a3	1.71	44.8	2T	0.09	17.2	41.4	32.6	26.9	2.41	16.5	0.68	24.3	1.1
a4	3.58	53.0	1T	0.13	11.4	30.4	23.3	18.5	2.67	15.3	0.72	21.1	0.8
a5	3.24	54.6	2T	0.08	8.92	28.5	26.2	15.6	3.19	12.2	0.73	16.7	0.8
Mean: 20.6 $\pm$ 3.1 Ma, 15% standard deviation													
<i>Note</i> : Rows in <i>italics</i> indicate grains that are outliers from the main population and not included in averages. Cor.—corrected; elev.—elevation.													
<sup>a</sup> Mean and 1 $\sigma$ standard deviation of corrected dates reported for samples with <20% standard deviation. No mean reported for samples with >20% standard deviation.													
<sup>b</sup> Equivalent spherical radius (r), the radius of a sphere with the same surface area to volume ratio.													
<sup>c</sup> Type of grain terminations: 2T—whole grain; 1T—one tip broken off; 0T—both tips broken off.													
<sup>d</sup> eU: effective uranium concentration, weights U and Th for their alpha productivity, compiled as [U] + 0.235 * [Th].													
<sup>e</sup> F <sub>T</sub> is alpha-ejection correction of Ketcham et al. (2011).													
<sup>f</sup> Analytical uncertainty based on U, Th, He, and grain length measurements.													

before being at the surface again (Table 1.2) by the present. Prior to thermal modeling, the apatite data for each sample was binned into two groups, those with eU values <30 ppm and >30 ppm. For each eU bin, the mean U, mean Th, mean Sm (all units in ppm), mean spherical radius ‘r’ ( $\mu$ m), mean uncorrected He date (Ma) was input. The uncertainty used was the standard deviation of each bin if it was >10% of the bin mean. If it was <10%, then 10% of the mean for the bin was applied. The  $\alpha$ -ejection was corrected in HeFTy after Ketcham et al. (2011). We used the radiation damage accumulation and annealing (RDAAM) He kinetic model (Flowers et al., 2009) in HeFTy version 1.9.3 and attempted 500 good-fit tT paths for all models.

## Results

We report 89 individual AHe dates from seventeen samples with 3-6 grains per sample (Table 1). Thirteen of the samples exhibit 20% or less dispersion and have mean dates ranging from 7.9  $\pm$  1.4 Ma to 55.2  $\pm$  10 Ma, while two samples from Silver City, one from Bogus Basin, and one from Challis have sample dispersions greater than 20% (Table 1). Figures 3 and 4 show AHe date vs eU plots for all samples, with individual grain dates plotted with their 2 $\sigma$  analytical uncertainties. For most samples, the date does not seem to vary strongly with eU. Average dates for samples from the Silver City and Bogus Basin transects are Eocene and Oligocene, while the Challis transect is younger with Miocene dates. Dates from Owyhee front transect are remarkably uniform Eocene dates that are some of the oldest in the dataset. The sample dates show an unexpected relationship with elevation in the Owyhee Mountains where the youngest dates are at high elevations and the oldest

TABLE 2. Thermal History Model Input for Southwest Idaho Samples

1. Thermochronologic data			
Samples and data used in simulations			
Sample	Rock Type	eU bins for AHe data <sup>a</sup>	Emplacement age used in model
<b>Owyhee Mtns.</b>			
KW-10-18-02	Kg (Cret. 2-mica granite)	<30ppm (7 grains)	75 ± 2 Ma (Gaschnig et al., 2010); box range: 90-65 Ma
KW-10-18-03	Kg	<30ppm (5 grains), >30ppm (1 grain)	
KW-10-18-05	Kg	<30ppm (4 grains)	
KW-10-18-07	Kg	<30ppm (5 grains)	
KW-10-18-10	Kg	>30 ppm (6 grains)	
OW-19-04	Kg	<30ppm (3 grains), >30ppm (2 grains)	
OW-19-06	Kg	<30ppm (2 grains), >30ppm (1 grain)	
OW-19-07	Kg	>30ppm (5 grains)	
<b>Boise Mtns.</b>			
BOI-19-01	Kg	>30ppm (5 grains)	47 ± 2 Ma (Gaschnig et al., 2010); box range: 52-42 Ma
BOI-19-02	Kg	<30ppm (2 grains), >30ppm (3 grain)	
BOI-19-03	Kg	<30ppm (4 grains)	
BOI-19-06	Kg	>30ppm (5 grains)	
BOI-19-07	Tei (Eocene granodiorite)	<30ppm (5 grains), >30ppm (1 grain)	
BOI-19-11	Tei	<30ppm (5 grains)	
BOI-19-13	Tei	<30ppm (3 grains), >30ppm (2 grains)	
<b>AHe data treatment: Dates, uncertainties, and other relevant constraints</b>			
Treatment: Samples were binned into groups with similar eU values, and the mean of each group was modeled.			
He dates (Ma): Mean uncorrected He date of each bin.			
<sup>a</sup> Ejection correction in HeFTy using Ketcham et al. (2011).			
Error (Ma) applied in modeling: The 1 $\sigma$ sample standard deviation of each bin was applied if $\geq 10\%$ . If <10%, then 10% was applied.			
r ( $\mu\text{m}$ ): Mean equivalent spherical radius of each bin.			
eU (ppm): Mean U and Th for each bin.			
eU zonation: None assumed.			
<b>2. Additional geologic information</b>			
Constraint	Explanation and source		
<b>All rocks (Cretaceous and Eocene)</b>			
(1) >120 °C at time of emplacement	Granitoid rocks emplaced as hot magma.		
(2) 10 ± 5 °C at present day	Present-day approximate surface temperature.		
<b>Owyhee Kg rocks</b>			
(1) 0-40 °C at ~20-16 Ma	Temp. range allows for arrival at the surface and formation of erosional unconformity.		
(2) 0-120 °C at ~16-10 Ma	Allows for possible heating during eruption and surface flow of basal volcanic units starting ~16.5 Ma (e.g., Tsc, Tlb) (Bonnichsen et al., 2008; Panze, 1975), or heating related to burial from volcanics or elevation of geotherm.		
<b>3. System- and model-specific parameters</b>			
He kinetic model: RDAAM (radiation damage accumulation and annealing model; Flowers et al., 2009).			
Statistical fitting criteria: Goodness of fit (GOF) values >0.5 for "good" fits. >0.05 for "acceptable" fits. The good fits also must have a minimum GOF of 1/(N+1) where N is number of statistics used (Ketcham et al., 2005).			
Modeling code: AHe uses HeFTy v1.9.3.			
Number of time-temperature paths attempted: 500 good-fit paths for all models.			

dates are from elevation samples along the Owyhee range front. There is a more typical relationship of increased age with elevation seen in samples from the Challis transect.

For the Silver City transect samples, the mean AHe dates range from 26.5-47.1 Ma. The tT models for these samples have similar acceptable and good fit paths, with all showing a cooling phase in the late Eocene to Oligocene (Fig. 1.3B). AHe data is best constrained between ~35-100 °C, so the trajectory and time frame of tT paths in that temperature range is key for interpreting the thermal models. The Owyhee front samples are 0-300 m lower in elevation than the lowest Silver City transect sample and have mean AHe dates that range from 42.4-49.3 Ma. The tT models for Owyhee front samples show an earlier cooling phase, ca. 55-42 Ma (early Eocene), while the Silver City transect samples have a cooling phase ca. 45-25 Ma, with latest cooling (~30-25 Ma) in the two highest elevation samples. All Owyhee samples allow for reheating in the mid-Miocene, some samples up to 100°C, but do not require it (Fig 3B). The Bogus Basin transect samples in the Boise Mountains have AHe dates very similar to the Owyhee samples but with a different spatial pattern. Bogus Basin tT

models show a cooling phase ca. 55-30 Ma, with mean cooling dates between 31.2-55.2 Ma, but with the youngest at the range front and increasing age with elevation. The highest elevation sample alone is anomalously young (BOI-19-06, 38.2 Ma), reminiscent of the pattern seen in the Owyhee Silver City transect (Fig. 1.4B). The Challis transect samples have mean cooling dates from 7.9-20.6 Ma, and their tT models have nearly identical trajectories as the Bogus Basin samples, but shifted 30 m.y. younger, with a cooling phase ca. 22-8 Ma (Miocene). The Challis samples show a clear positive correlation between cooling date and elevation (Fig. 1.5).

A similarity across all samples regardless of location is the lack of significant correlation between AHe date and eU (Figs. 3A, 4A). This absence of date-eU correlation suggests none of the samples resided in the AHe PRZ for periods long enough for grains with higher radiation damage (and thus higher closure temperatures) to reflect older dates than grains with less radiation damage, implying that all samples likely experienced rapid cooling. This is reflected in the shape of the modeled tT paths, which all show extremely steep paths through the apatite PRZ (Figs. 1.3B, 1.4B).

## **Discussion**

### **Paleogene Exhumation and Topography**

The AHe data and thermal models for all Cretaceous samples indicate rapid cooling of the southern Idaho batholith and Silver City pluton in the Eocene to early Oligocene (Figs. 1.3, 1.4). Southern batholith cooling dates from AFT and ZFT (Sweetkind & Blackwell, 1989), ZHe (Fayon et al., 2017), and this study all have a remarkably similar ~25 m.y. range in the Eocene, despite the ~250-70 °C spectrum of closure temperatures of these thermochronometers (Fig. 1.1). This suggests a phase of rapid cooling and exhumation to near surface temperatures through the Eocene. The Silver City transect in the Owyhee Mountains displays an inverted date-elevation relationship, with younger dates at high elevations and the oldest dates at low elevations (Fig. 1.5A). Such a relationship can occur when topographic relief decreases (Braun, 2002) and we take this to indicate decay of relief with decreasing erosion rates post-Eocene. These results are consistent with the picture of a

high relief, rapidly exhuming landscape in the Idaho batholith during the Eocene followed by decreased relief.

We calculated estimates of Eocene exhumation using several assumed geothermal gradients and the amalgamated low temperature thermochronometry dataset. In the central batholith, away from the major river canyons, most dates from low temperature thermochronometers are Eocene (Fig. 1.1), implying  $\sim 180$  °C of cooling during this period. The Challis magmatic event affected this region and continued for  $\sim 10$  m.y. in Idaho (e.g., Fayon et al., 2017), resulting in elevated regional geothermal gradients in the Eocene. An unusually high gradient of  $75$  °C/km would only require  $\sim 2.5$  km of exhumation to cause this much cooling. Discounting Challis effects, a more typical geothermal gradient of  $25$  °C/km would indicate nearly 8 km of exhumation. However, we favor a moderately high geothermal gradient of  $40$  °C/km. This is the present-day gradient from geothermal well studies (Blackwell et al., 2011) and was used for estimating Idaho batholith exhumation magnitude by Fayon et al. (2017). Using a gradient of  $40$  °C/km, a rock unit passing from  $250^\circ$  to  $70^\circ$  in the crust would require  $\sim 4.5$  km of unroofing during Eocene to early Oligocene time. Over a period of 25 m.y., this equates to an exhumation rate of  $0.18$  km/my. This matches well with the exhumation rate estimated from the tT paths of several of our thermal history models ( $\sim 0.2$  km/my), assuming our models are representative of cooling from  $150$ - $50$  °C. It is possible that some of the cooling during this time represents post-magmatic cooling after the period of Challis magmatism, as plutonism can affect thermochronometry dates from surrounding rocks (Murray et al., 2018). Such effects are complex but would mean that the true exhumation magnitudes would be lower than those calculated with simple geothermal gradients. However, the Challis-aged Sawtooth batholith was emplaced at  $\sim 5$  km depth (Gaschnig et al. 2010) showing that parts of the batholith resided at  $\sim 5$  km crustal depths in the Eocene and have since been exhumed.

Focused Eocene cooling dates from our Cretaceous samples indicate significant rock uplift, which, broadly speaking, could be driven by rapid surface erosion or extensional exhumation. There is ample evidence for rapid erosion of the Idaho batholith in the Eocene. Detrital sediment studies of Eocene basins in Oregon, California, and Wyoming have found significant volumes of Idaho batholith sediment (e.g., Dumitru et al., 2013; Chetel et al.,

2011; Heller et al., 1985), and Challis volcanic ages were found in detrital sediments in northeastern Nevada basins (Canada et al., 2019), implying sediment transport from Idaho to all over the US Cordillera. Thus, the exhumation rates are at least partly driven by rapid surface erosion. Extension was occurring in Idaho during the Eocene, but our study area is removed from any of the major core complexes (e.g., Stevens et al., 2017). The nearest extensional structure is the trans-Challis fault zone (TCFZ, Fig. 1.1; Kiilsgaard & Lewis, 1983; Bennett, 1986; Johnson et al., 1988; Breckenridge et al., 2003), a zone of major regional high-angle northeast-trending faults that stretch across central Idaho from the edge southern Idaho batholith into Montana. Though a major regional feature, there is no evidence of major faults near our sample transects in the Boise Mountains, and there is no obvious evidence for major differences in exhumation depths across the structure. While there may have been enhanced exhumation and surface uplift in the footwalls of these structures in the Eocene, it is not directly reflected in the thermochronology (Fig 1.1; Fayon et al., 2017; Sweetkind & Blackwell 1989). While both erosion and extension played a role in rock exhumation and generation of topographic relief in the southern Idaho batholith and both processes could be reflected in our AHe dates, it is clear that rapid erosion of the batholith was occurring at that time.

High erosion rates in the Eocene is suggestive of an active landscape with steep slopes and high relief. In general, high rock uplift and erosion rates correspond to steeper slopes and higher relief landscapes (e.g., Montgomery & Brandon, 2002; Wobus et al., 2006). We suggest that high Eocene slopes and relief were due to surface uplift in southern Idaho, which is supported by various paleotopographic studies across the western Cordillera. Comparisons of leaf physiognomy from modern vegetation of known climates with that of Eocene and Oligocene fossil leaves from the northwestern U.S. suggest the paleoelevation in central Idaho was higher than today by up to 4 km or more (Wolfe et al., 1998).  $\delta^{18}\text{O}$  values of calcites in southwestern Montana and north-central Idaho decrease by 7-10‰ between ~50-47 Ma, likely as a result of a 2.5-3.5 km increase in elevation, contemporaneous with nearby Challis volcanism (Kent-Corson et al., 2006). Cassel et al. (2014) reconstructed a paleotopographic profile across Nevada using  $\delta\text{D}$  values of meteoric water preserved in volcanic glass, showing a high, broad orogen that existed from the Eocene to Oligocene that maintained higher elevations than modern topography, reaching 3500 m in the late

Oligocene. Stable isotope data (paleosol carbonate  $\delta^{18}\text{O}$  and  $\delta^{13}\text{C}$ ) from southwestern Montana (Schwartz et al., 2019) show that surface elevations progressively increased from

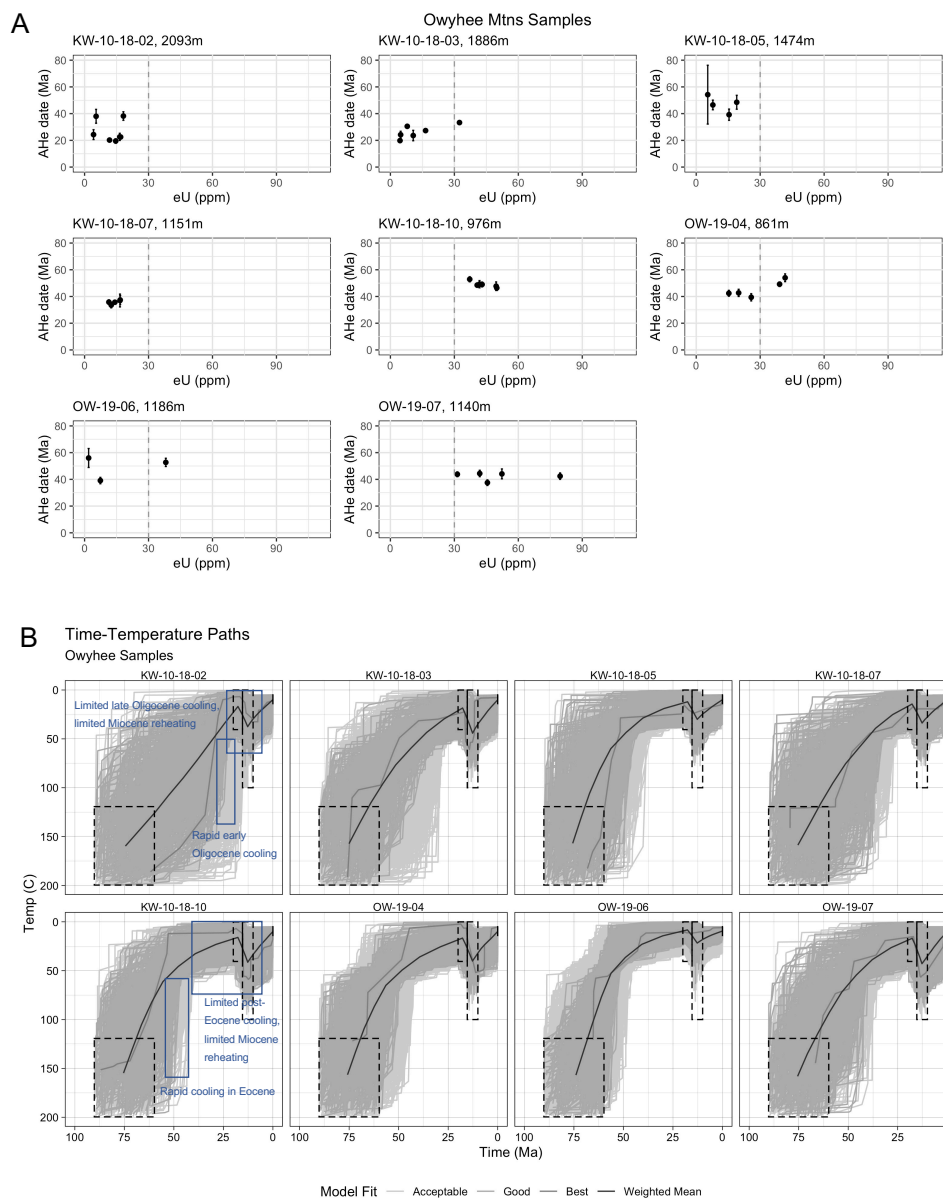


**Figure 1.3.** (A) AHe date-eU plots for all Owyhee samples with  $\leq 30\%$  standard deviation of dates. Each is labeled with sample name and elevation. Vertical dashed line marks the divide between the two eU bins used for HeFTy modelling (see Table 1.2). Errors are plotted as the  $2\sigma$  analytical uncertainty, and in some cases are smaller than the symbol. (B) Thermal history modeling results for the Owyhee samples in A. The tT plots show the thermal history constraints as dashed boxes, the weighted mean path in black, the best-fit path in dark gray, good-fit paths in gray, and acceptable-fit paths in light gray. Additional details of model inputs and their rationale are in Table 1.2. Blue boxes illustrate how these tT paths are interpreted for KW-10-18-02 (Silver City transect) and KW-10-18-10 (Owyhee front transect).

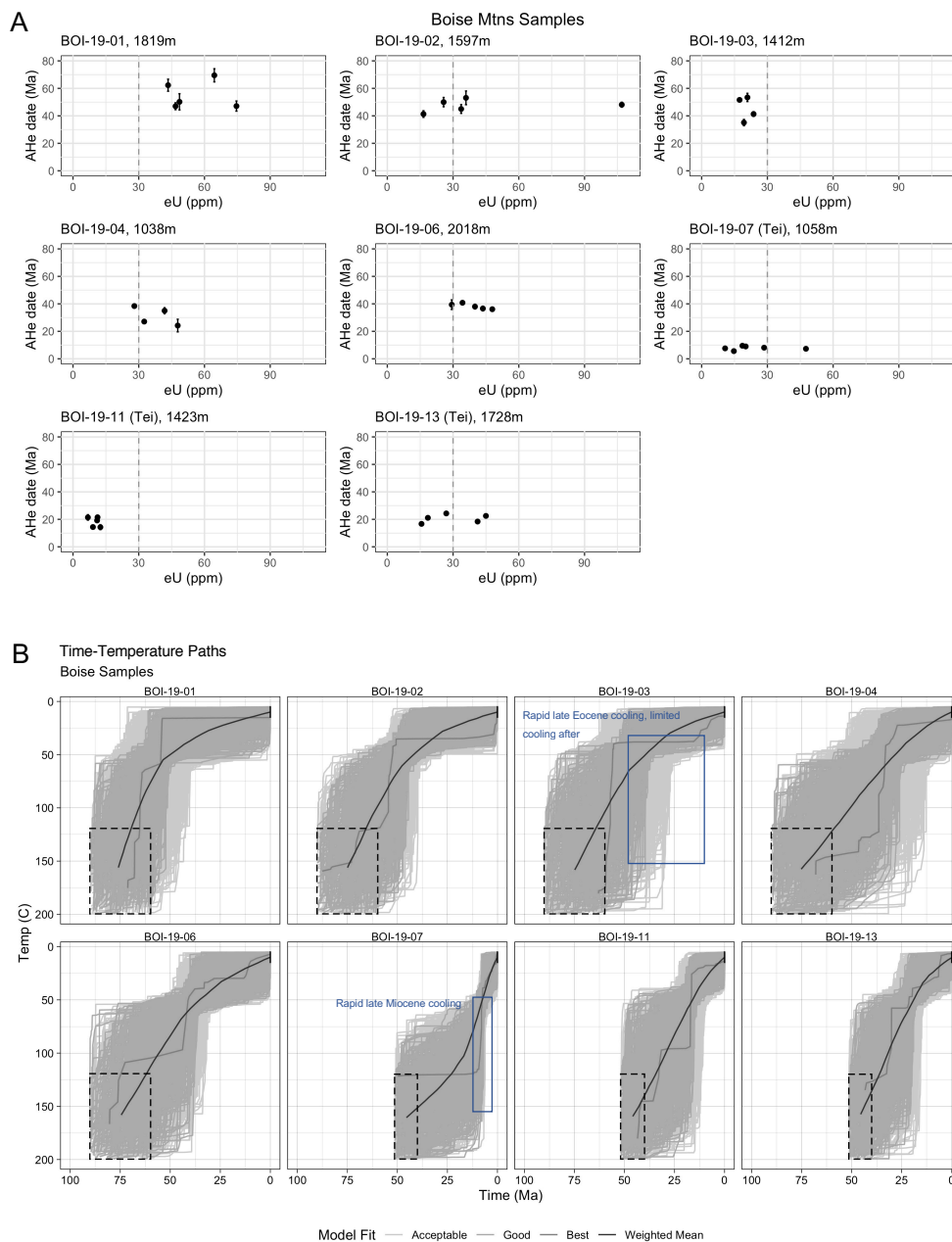


**Figure 1.4.** (A-B) AHe date-eU plots and thermal history modeling results for all Boise samples. Symbology same as Figure 3. Blue boxes illustrate how these tT paths are interpreted for BOI-19-03 (Bogus Basin transect) and BOI-19-07 (Challis transect).

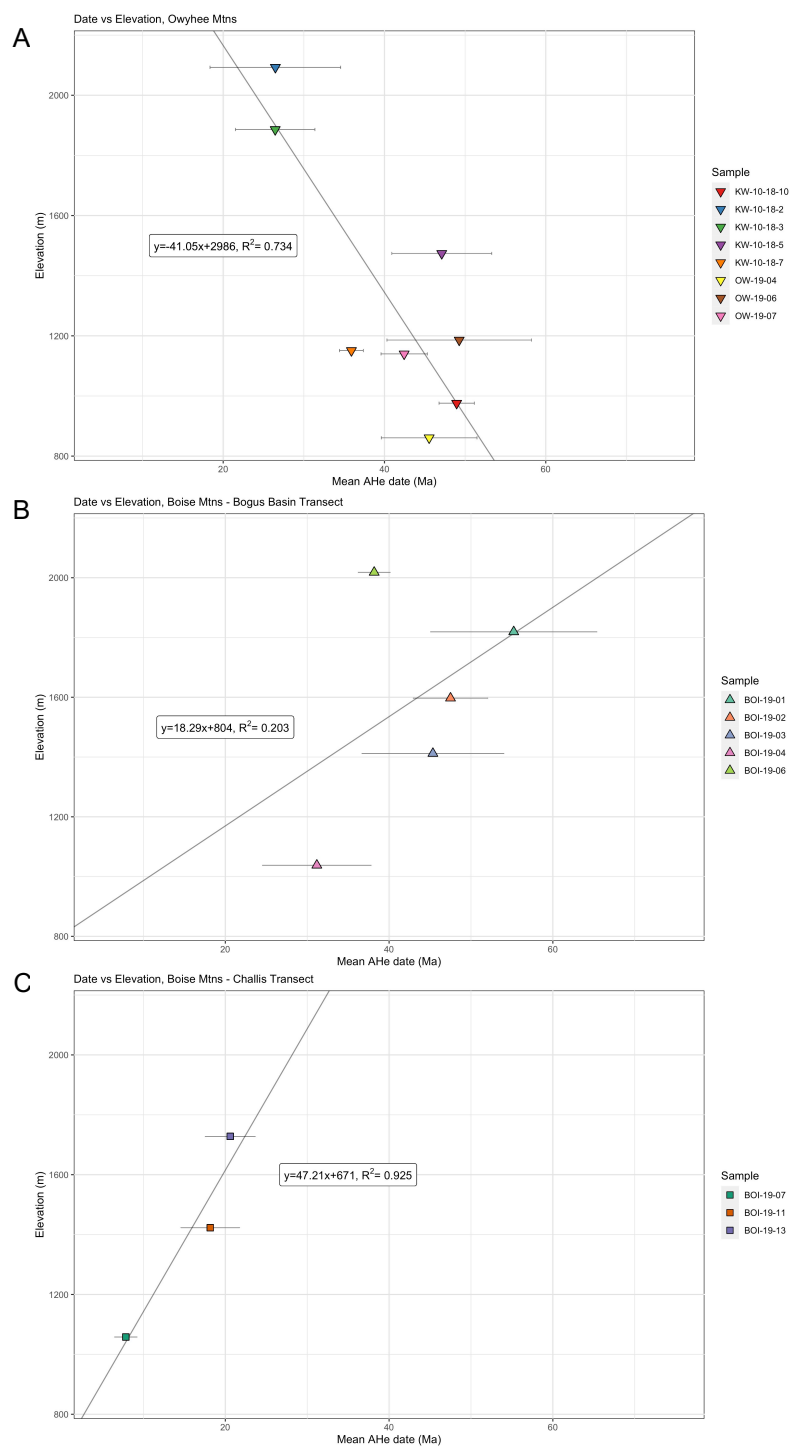


**Figure 1.5.** (A-C) Date-elevation profiles for all transects (Silver City and Owyhee front are combined). Each plot shows the best-fit line for the data, with the slope, intercept, and  $R^2$  value labeled. The date-elevation relationship of the Owyhee samples has an inverted slope, which can occur when surface topography relief is decreased (Braun, 2002).

Late Cretaceous to middle Eocene time, with peak elevations  $\geq 4$  km ca. 50 Ma following thermal uplift of the lithosphere. Accelerated erosion of the batholith in the Eocene may have been enhanced due to higher temperatures and precipitation. The Eocene represents the apex of greenhouse climate in the Cenozoic, likely the result of increased volcanic CO<sub>2</sub> emissions during the Paleocene and Eocene epochs, with warmer and wetter climates at both high and low elevations (Zachos et al., 2008; Snell et al., 2011). Higher rainfall and temperatures contribute to increased rates of chemical weathering and transport of eroded material. However, evidence for high topography and focused exhumation in the Idaho batholith suggest that surface uplift maintaining steep slopes and active erosion was key for our observations. Evidence from our data for post-Eocene relief reduction also imply that there was a previously high relief landscape.

We interpret from our data that the high relief topography built through the Eocene decreased during the Oligocene. This is supported by the unexpected date-elevation pattern of the Owyhee Mountains samples. The pattern is unanticipated because the youngest dates are at the highest elevations and the oldest dates are at lower elevations along the range front (Figs. 1.2, 1.5). An explanation for this can be found by exploring date-elevation relationships. The slope of an AHe date-elevation relationship is sensitive to relative surface relief changes, and the date-elevation slope often becomes inverted if the amplitude of relief decreases (Braun, 2002). This could be explained by a topographically high region experiencing accelerated erosion for tens of millions of years through the Eocene and Oligocene followed by a reduction in exhumation and erosion rates, resulting in overall decreased relief (Fig. 1.6). This is also supported by the apparently fewer Oligocene cooling dates in the batholith compared to the Eocene epoch. The shape of the thermal model  $tT$  paths for the Cretaceous samples show extremely steep paths between 150-50 °C then an immediate near-horizontal slope until reaching surface temperature, indicating rapid exhumation in the Eocene followed by much slower exhumation rates in the Oligocene and later (Fig. 1.3). Another possible explanation for the younger high elevation dates is that those samples have been partially reset in the Miocene by rhyolite and basalt flows that were deposited directly on exposed granite bedrock. However, this is unlikely to explain the pattern of dates seen in the Owyhees, because granite at low elevations was also exposed to volcanic flows, but the range front samples have uniformly mid-Eocene cooling dates. Partial

resetting of the AHe system due to conductive heating, while variable due to physical parameters and exposure time, is likely only an issue within 40-100 m of bedrock/volcanic contacts (Karlstrom et al., 2019). Thermal modeling constraints for the range front and Silver City transect samples in the Owyhee Mountains allowed for up to 100 °C of reheating during mid-Miocene volcanism, however none of the good-fit paths in any sample reached above 80 °C and many show no reheating, suggesting samples are unlikely to be strongly reset. Thus, considering these two possible explanations, we choose to interpret the inverted date-elevation relationship of Owyhee samples to the Oligocene decay of a high relief mountain range or incised plateau in Idaho.

Our data present a picture of a high relief, rapidly eroding landscape in the Eocene, followed by relief reduction. The rapid cooling seen through the Eocene-early Oligocene provides further evidence for an incised mountain range or high plateau (e.g., Byerly et al., 2016; Fayon et al., 2017), and supports Eocene detrital studies (e.g., Canada et al., 2019; Dumitru et al., 2013; Chetel et al., 2011; Heller et al., 1985). Our new AHe dataset sits well in the broader scale climatic and tectonic context during this period of post-Laramide slab delamination – sweeping magmatism, regional uplift and extension, and significant erosion and sedimentation across the western Cordillera, all amidst the highest global temperatures of the Cenozoic Era. Our evidence supports enhanced exhumation and erosion of a high relief landscape in Idaho that is concurrent with Farallon slab rollback and regional Challis magmatism.

### **Miocene Extension**

The Cretaceous samples from the Owyhee Mountains and the Boise Mountains demonstrate that the cooling and exhumation of the mountainous flanks of the WSRP occurred between 55-26 Ma, well before Miocene WSRP formation. Our AHe data from the Owyhee front transect show uniformly mid-Eocene cooling dates with no apparent spatial variability along strike (NW-SE). The Boise front sample is younger than any Owyhee front sample, but also predates the development of the WSRP (Fig. 1.2). The map pattern of granite in the Owyhee Mountains show that granite bedrock was at the surface with some relief in the Miocene prior to early stages of rifting, yet there are no obvious basin-bounding faults in the field. The Boise Mountains, however, do have obvious range front fault

escarpments and evidence of major Tertiary faulting (Breckenridge et al., 2003). The lowest elevation Bogus Basin sample [BOI-19-04] is the youngest in that transect and over 10 Ma younger than any Owyhee front sample, which may indicate more fault-related exhumation occurred on the north flank of the WSRP. Challis transect samples in the Boise Mountains experienced rapid cooling in the Miocene, which may be related to base level lowering during WSRP extension and river incision into the interior of the batholith.

However, the utter lack of any Miocene or younger cooling dates in the WSRP footwalls limits the amount of range-bounding fault-related exhumation that occurred during rifting. On the Owyhee side, it is clear that samples sitting in the PRZ prior to faulting have not been exhumed to the surface, limiting the samples at the range front to  $<50^{\circ}\text{C}$  prior to rifting. On the Boise Mountains side, this may also be true, but the slightly younger samples at the base of the Bogus Basin transect may denote the very top of the PRZ, meaning that samples may have been in the  $50\text{-}70^{\circ}\text{C}$  range. Using a range of geothermal gradients, it is possible to calculate a range of depths to the  $50$  and  $70^{\circ}\text{C}$  isotherms to determine the maximum exhumation possible in the case of each geothermal gradient. Assuming the exhumation is fault driven, and ignoring footwall rotation and isostatic rebound, then the maximum exhumation amount can be considered the maximum fault throw on range-bounding faults. Using a geothermal gradient range from a relatively low  $25^{\circ}\text{C}/\text{km}$  to a high gradient of  $100^{\circ}\text{C}/\text{km}$ , the maximum flank exhumation and fault throw that occurred on range-bounding faults is between  $0.7\text{-}2.8$  km. However, considering the geotherm was likely elevated during Miocene volcanism, the maximum exhumation/fault throw is more likely to fall into the middle to lower end of that range. We then used moderate to steep normal fault dip angles ( $40^{\circ}\text{-}70^{\circ}$ ) and our calculated range of fault throw to evaluate extension magnitudes. The highest fault throw ( $2.8$  km) at a dip of  $40^{\circ}$  yields just over  $3$  km of extension, or about  $5\%$  of the WSRP  $60$  km width. A throw of  $0.7$  km yields  $0.25\text{-}1$  km of extension, barely  $1\%$  of the basin width. If extensional faulting is the main mechanism causing subsidence in the basin, Wood and Clemens (2002) calculate that about  $10\%$  extension is needed to account for the basin volume. This therefore suggests that at least half and possibly more of the extension and subsidence has not occurred on the basin-bounding faults.

This limit on basin-bounding flank exhumation and extension lends credence to a model of extension in the WSRP accommodated by intrabasinal structures and invasion by mafic intrusives. High seismic velocities indicate that the WSRP has been heavily intruded by dense material such as basalts and a large positive Bouguer anomaly in the axis is consistent with a large, 20-30 km-wide central basin horst (Hill & Pakiser, 1967; Mabey, 1976; Wood & Clemens, 2002; Shervais et al., 2011; Kessler et al., 2017). The basement profile is often modeled as a series of basaltic horsts bounded by steep NW-trending faults across the WSRP (Barton & Ratchford, 2020; Arney et al., 1982; Shervais et al., 2002). Thus, intrabasinal faulting and basalt dike associated with the CRBG and Yellowstone plume may be responsible Miocene extension in the WSRP crust. This mode of strain accommodation via magmatic intrusion and faulting is seen in the actively deforming “magmatic segments” of the Main Ethiopian Rift (MER), the northernmost part of the East African Rift system. Magma intrusion into the mid- to upper crust in the MER triggers faulting and dike intrusion into the brittle upper crust (Casey et al., 2006). This is also typical of the basins formed in eastern North America during early Mesozoic continental rifting of Pangea (Philpotts, 1992; Pe-Piper et al., 1992). Cooling and contraction of the intruded basalts would also contribute to subsidence in the WSRP. The average subsidence rate of normal young (<70 Ma) seafloor is  $\sim 320 \text{ m Ma}^{-1/2}$ , based on a half space cooling model (Korenaga & Korenaga, 2008; Turcotte & Schubert, 1982; Parsons & Sclater, 1977), which may be too simplistic for continental areas like the WSRP, but it provides a first order estimate for the maximum amount of subsidence from cooling. If we assume basalt magmatism in the WSRP occurred during CRBG volcanism at  $\sim 16 \text{ Ma}$ , then the half space cooling model predicts  $\sim 1280 \text{ m}$  of subsidence. If basalt emplacement is temporally correlated with Yellowstone plume activity at the Bruneau-Jarbidge eruptive center  $\sim 12 \text{ Ma}$ , then this model predicts  $\sim 1108 \text{ m}$  of subsidence. However, the  $\sim 2\text{-}3 \text{ km}$  sediment thicknesses in the WSRP basin still require some fault driven subsidence.

This picture of limited flank exhumation, no obvious along-strike variability in exhumation on the Owyhee front, and basalt dike accommodating extension and subsidence can be used to evaluate the three models for WSRP development. The first model is extension driven by lithospheric stresses caused by the eruption of CRBG and it predicts a NW to SE pattern of extension initiation and footwall exhumation coincident with peak

CRBG activity ca. 16 Ma. There is no apparent along-strike age difference in the Owyhee front transect samples to indicate any NW-SE spatiotemporal pattern of faulting. Challis transect cooling dates span 20-8 Ma and may reflect base level lowering during basin extension, but they do not specifically pinpoint any particular event ca. 16 Ma. The second model is that extension is driven by thermal tumescence of an upwelling the Yellowstone mantle plume tail, particularly near the Bruneau-Jarbridge area ca. 12-10 Ma. It predicts a SE to NW pattern of faulting, with greatest faulting and exhumation near the eruptive center. Though no spatio-temporal pattern of faulting can be derived from our range front transect data, many of the faults mapped on the SE end of the WSRP are dated between ~11-10 Ma (Wood & Clemens, 2002; Clemens & Wood, 1993). The third model posits that the WSRP is not correlated with CRBG or Yellowstone hotspot activity, but that it is an unusually wide Basin and Range graben with clear basin-bounding faults, with fault initiation and flank exhumation that is uniform along the faults or maximal in fault centers (e.g., Ellis & Barnes, 2015). However, our AHe dates limit Miocene flank exhumation, thus the importance of WSRP extension accommodated by intrabasin faulting and basaltic intrusions cannot be overstated. The limited extent and magnitude of throw of range front faults and importance of magmatic extension in the WSRP is a style that differs from the typical amagmatic Basin and Range horst-and-graben extension dominant south and east of the WSRP (Eaton, 1982). Though our AHe data cannot constrain the timing of extension to correlate with CRBG eruptions or Yellowstone plume proximity specifically, due to the importance of basaltic magmatism, limited basin-bounding fault throw, and differences in physiography and style from Basin and Range structures, we favor WSRP formation due to intrabasin faulting and magmatic intrusions related to regional Miocene volcanism (Fig. 1.6; e.g., Camp & Ross, 2004; Glen & Ponce, 2002; Shervais et al., 2002, Wood & Clemens, 2002).

### **Miocene Landscape Rejuvenation and Incision**

Our transect in Eocene Challis granite above the MFB River has cooling dates that span the Miocene (20.6-7.9 Ma), reflecting a cooling history different from the samples from the WSRP flanks. The Challis samples exhibit a positive date-elevation relationship, with the oldest dates at higher elevations and the youngest date in the river canyon (Fig. 1.5C). In a simplistic sense, the slope of this could reflect the exhumation rate in the Miocene (Fig. 1.6),

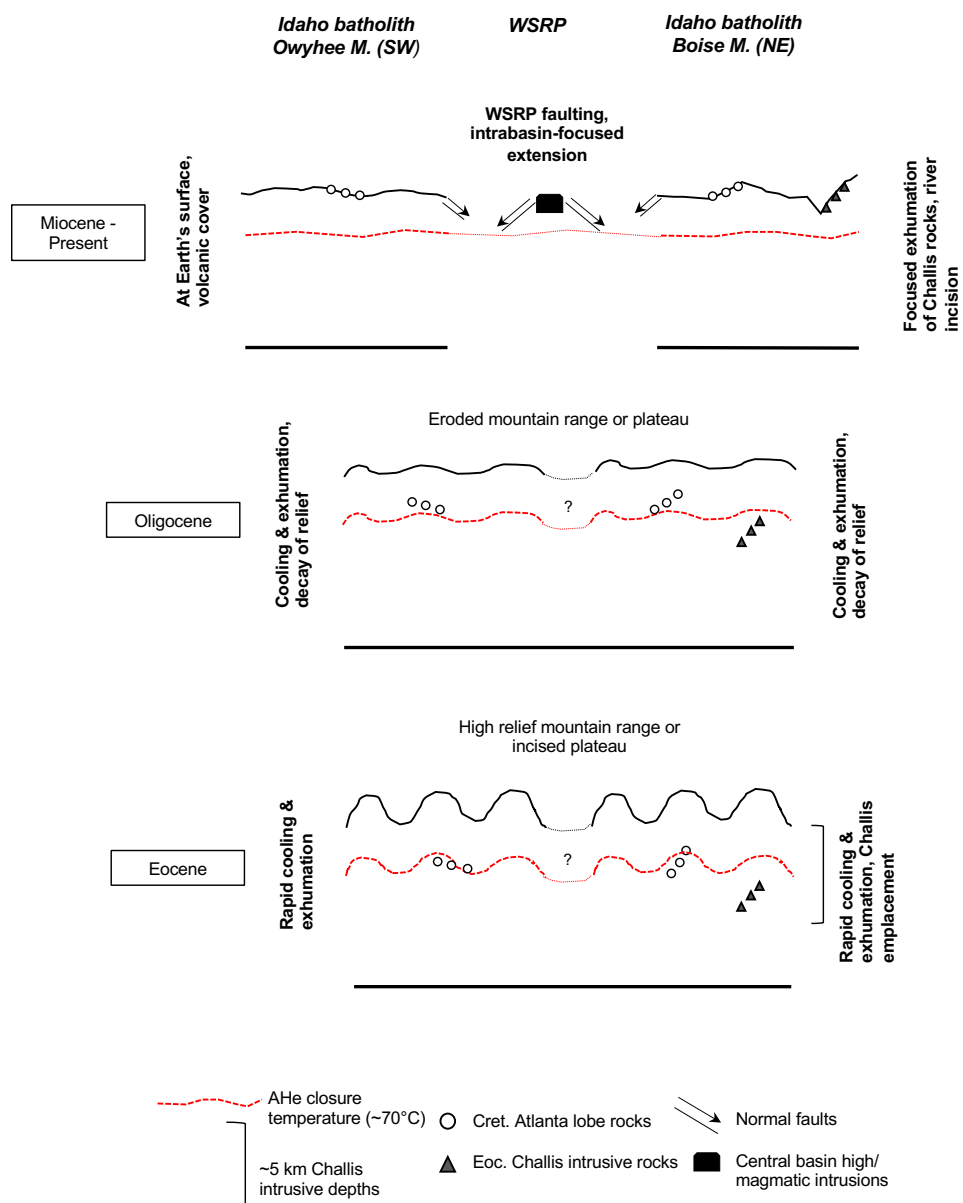


**Figure 1.6.** Schematic models showing crustal cross sections across the WSRP for the Eocene, Oligocene, and Miocene-Present, illustrating the emplacement of Challis intrusive rocks, exhumation and topographic evolution of the southern Idaho batholith, and development of the western Snake River Plain rift, as inferred from our new AHe cooling dates. Cret. – Cretaceous, Eoc. – Eocene.

however, in rapidly eroding environments, the 70 °C AHe closure isotherm is perturbed by surface topography and the slope is affected by changes in relief (Braun et al., 2002) so it is not likely that this slope reflects the true exhumation rate. The positive slope does indicate constant or increasing relief in the Challis rocks incised by the MFB River, compared to the decay of relief (and inverted slope) seen in the Owyhee date-elevation relationship (Fig. 1.5A). Challis inverse models show rapid cooling and exhumation through the AHe PRZ, and relatively fast cooling to surface temperatures as well (Fig. 1.4B). We interpret our Challis transect data to reflect incision of the MFB River canyon and increasing relief.

Evidence of Miocene landscape rejuvenation in the Idaho batholith include studies of river incision in the batholith. A study of  $^{10}\text{Be}$  cosmogenic radionuclide concentrations in river sediment by Larimer et al. (2018) shows that incision rates increased from  $\sim 0.05$  mm/yr to 0.12 mm/yr, initiated ca. 9.5 Ma and which persist to present time. This study observed that Idaho batholith topography consists of patches of low-slope landscape dissected by steep canyon incision, echoing much earlier workers in the batholith (e.g., Lindgren, 1904; Umpleby, 1912; Blackwelder, 1912) who recognized central Idaho as an incised high plateau, characterized by deep canyons separated by even-crested divides. Mitchell & Yanites (2019) noted increasing knickpoint elevations and incision depths (800-2,200 m and 300-1,200 m respectively) from north to south in the batholith. Both studies attribute this rejuvenation to surface uplift driven by plume-lithosphere interaction and base level fall from drainage of Pliocene Lake Idaho down to the proto-Snake River. Previous thermochronology studies in the area found similar patterns of cooling as our data, with late Miocene AFT dates in Eocene Challis granitic samples from incised river canyons in the Boise Mountains (Sweetkind & Blackwell, 1989) and AHe dates from Challis plutons the Pioneer-Boulder Mountains east of the Idaho batholith that indicate as much as a 3-fold increase in exhumation ca. 11.5-8 Ma (Vogl et al., 2014).

We suggest three explanations for increased Miocene incision in the southern Idaho batholith. First, uplift in the highlands related to Yellowstone plume-lithosphere interaction (e.g., Vogl et al., 2014; Larimer et al., 2018; Mitchell & Yanites, 2019). This might be accomplished through buoyant support from the plume (Pierce & Morgan, 1992), or perhaps flexural isostasy due to the region's suspected lithospheric loss, proposed by Larimer et al.

(2018). Second, base level fall in the lowlands via either subsidence of the WSRP during the mid-Miocene or lake level fluctuations in Lake Idaho during the late Miocene to Pliocene (e.g., Swirydczuk et al., 1979). And third, increased erosional exhumation related to climate change influence. The warmer climate of the mid-Miocene climatic optimum (MMCO, ~17-15 Ma; Zachos et al., 2001, 2008) promoted a prolific temperate broadleaved forest in Idaho (e.g., Leopold & Denton, 1987) with small lacustrine and swamp environments associated with black shale and coal layers in the lowest WSRP basin sediments (Love et al., 2020). Surface uplift related to the Yellowstone plume and base level fall in the WSRP, whether related to basin subsidence or Lake Idaho fluctuations, all coincide with the range of Miocene cooling ages from our Challis transect samples, but it is not really possible to differentiate between them based on our data. Warmer and wetter climate associated with the MMCO might have enhanced exhumation rates due to accelerated erosion but is unlikely to have driven canyon incision on its own because it is shorter-lived than the span of rapid exhumation that we see. Additionally, rock uplift in the southern Idaho batholith seems to be maintained to present time. Mitchell & Yanites (2019) note the relatively rapid response of river steepness to the initiation and cessation of increased rock uplift or base level fall, meaning that a temporary pulse of increased uplift or base level fall create increased river steepness and after the signal's passage steepness values should decrease. Thus, the continuously high normalized steepness values of main drainages in the batholith suggest the factors driving rock uplift and increased incision during the Miocene are still active to present time. We interpret our AHe data to indicate increasing relief in the river canyons dissecting the Idaho batholith.

Our Challis cooling dates overlap with the depositional age of the Payette Formation, the stratigraphically lowest sedimentary unit in the WSRP and hydrocarbon source and reservoir rock, and the Chalk Hills Formation, which acts as the reservoir and sealing mudstone facies. Burial of the hydrocarbon source rocks likely began during the onset of Lake Idaho and the deposition of the Chalk Hills Formation, with additional burial and overburden accompanying deposition of the Glens Ferry Formation above (Love et al., 2020). New zircon U-Pb geochronology of volcanic interbeds and palynomorph biostratigraphy (Love et al., 2020) establish deposition of the Payette Formation starting at 16.39 Ma (coeval with the MMCO), and 9.00-7.78 Ma for the Chalk Hills Formation. The Payette Formation has ~460

m of sedimentary and volcanic interbeds and an additional ~460-600 m above the last volcanic units, deposited between ~17-12 Ma, followed by surface erosion. The Chalk Hills Formation is 300-520 m thick, deposited between ~9-6 Ma, with another subsequent erosional surface. The uppermost unit is the ~540 m thick Glenns Ferry Formation, which was initiated ~5 Ma and continued until drainage of Lake Idaho ~2 Ma. The deposition intervals and unit thicknesses suggest that deposition rates for these WSRP sediments were broadly similar (minimum 100 m/my), though each unit was punctuated by periods of non-deposition and erosion. Perhaps the highest deposition rate was during Payette sedimentation (~200 m/my). The abundant quartz, feldspar, biotite, and muscovite in the sediments indicate the nearby batholith and Challis intrusive rocks were the provenance source of the Payette Formation (Love et al., 2020). This correlates with our view that the southern batholith was experiencing increased exhumation, incision, and erosion in the Miocene. We propose that active extension and subsidence of the WSRP accommodated by magmatic intrusions and intrabasin faults was initiated in relation to CRBG volcanism ca. 16 Ma and this coincides with earliest basin sediment deposition. Our new AHe data provide further evidence of Miocene incision and relief generation in the mountain catchments north of the WSRP as well as deposition of Idaho batholith erosional detritus into the actively subsiding WSRP.

## Conclusions

New AHe dates from the Cretaceous granitoid rocks flanking the WSRP provides evidence of rapid cooling and exhumation of the southern portion Idaho batholith and the Silver City Pluton during the Eocene. These rapid exhumation rates and support the idea of a northern Nevadaplano or high relief mountain range in Idaho and uplift and exhumation associated with Farallon slab rollback and Challis magmatism. This high relief landscape supplied massive amounts of sediment to Eocene basins via rapid erosion and extension. We show evidence of post-Eocene decreased relief in southwest Idaho in the negative slope on date-elevation relationships in the Owyhee Mountains, indicating post-orogenic decay of these highlands. Eocene AHe dates from the mountain flanks of the WSRP indicate limited exhumation during Miocene basin formation. Because fault-related exhumation and therefore extension on the flanks of the WSRP must be limited, we interpret this to be evidence extension accommodated by faulting focused around a central basin high and related to basalt

dike intrusions. Focused exhumation at 20-7 Ma seen in the Challis transect relates to focused incision along the Middle Fork Boise River in the interior of the Boise Mountains due to relative base level fall or rock uplift due to plume-associated magmatism.

## References

- Abbey, A.L., and Niemi, N.A., 2020, Perspectives on continental rifting processes from spatiotemporal patterns of faulting and magmatism in the Rio Grande rift, USA: *Tectonics*, v. 39, e2019TC005635, doi: 10.1029/2019TC005635.
- Alsleben, H., Whetmore, P.H., and Gehrels, G.E., 2012, Detrital zircon ages in Palaeozoic and Mesozoic basement assemblages of the Peninsular Ranges batholith, Baja California, Mexico: Constraints for depositional ages and provenance: *International Geology Review*, v. 54, p. 93-110, doi: 10.1080/00206814.2010.509158.
- Andrews, G.D.M., Branney, M.J., Bonnicksen, B., and McCurry, M., 2008, Rhyolitic ignimbrites in the Rogerson graben, southern Snake River Plain volcanic province: Volcanic stratigraphy, eruption history and basin evolution: *Bulletin of Volcanology*, v. 70, p. 269–291, doi:10.1007/s00445-007-0139-0.
- Arney, B.H., and Goff, F., 1982, Evaluation of the hot-dry-rock geothermal potential of an area near Mountain Home, Idaho. United States. doi: 10.2172/5350339.
- Axelrod, D. I., 1997, Paleoelevation estimated from Tertiary floras: *International Geology Review*, v. 39, no. 12, p. 1124–1133, doi: 10.1080/00206819709465319.
- Barry, T.L., Kelley, S.P., Reidel, S.P., Camp, V.E., Self, S., Jarboe, N.A., Duncan, R.A., and Renne, P.R., 2013, Eruption chronology of the Columbia River Basalt Group, *in* Reidel, S., Camp, V., Ross, M., Wolff, J., Martin, B., Tolan, T., and Wells, R., eds., *The Columbia River Basalt Province*, GSA Special Paper 497, p. 45-66, doi: 10.1130/2013.2497(02).
- Barton, M., and Ratchford, M.E., 2020, Executive summary – petroleum geochemistry: Insights into the origin of natural gases and fluid hydrocarbons from the Western Snake River Plain, Idaho: Idaho Geological Survey Executive Summary.
- Becker, T.W., Faccenna, C., Humphreys, E.D., Lowry, A.R., and Miller, M.S., 2014, Static and dynamic support of western United States topography: *Earth and Planetary Science Letters*, v. 402, p. 234-246, doi: 10.1016/j.epsl.2013.10.012.
- Bennett, E.H., 1986, Relationship of the trans-Challis fault system in central Idaho to Eocene and Basin and Range extensions: *Geology*, v. 14, p. 481-484.
- Beranek, L.P., Link, P.K., and Fanning, C.M., 2006, Miocene to Holocene landscape evolution of the western Snake River Plain region, Idaho: Using the SHRIMP detrital zircon provenance record to track eastward migration of the Yellowstone hotspot: *GSA Bulletin*, v. 118, p. 1027-1050, doi: 10.1130/B25896.1.
- Best, M. G., Christiansen, E. H., de Silva, S., and Lipman, P. W., 2016, Slab-rollback ignimbrite flareups in the southern Great Basin and other Cenozoic American arcs: A

distinct style of arc volcanism: *Geosphere*, v. 12, no. 4, p. 1097–1135, doi: 10.1130/ges01285.1.

Blackwelder, E., 1912, The old erosion surface in Idaho: A criticism: *The Journal of Geology*, v. 20, p. 410-414, doi: 10.1086/621986.

Blackwell, D., Richards, M., Frone, Z., Ruzo, A., Dingwall, R., and Williams, M., 2011, Temperature-at-depth maps for the conterminous U.S. and geothermal resource estimates: *GRC Transactions*, v. 35(GRC1029452).

Bonnichsen, B., Leeman, W.P., Honjo, N., McIntosh, W.C., and Godchaux, M.M., 2008, Miocene silicic volcanism in southwestern Idaho: Geochronology, geochemistry, and evolution of the central Snake River Plain: *Bulletin of Volcanology*, v. 70, p. 315-342, doi: 10.1007/s00445-007-0141-6.

Braun, J., 2002, Quantifying the effect of recent relief changes on age-elevation relationships: *Earth and Planetary Science Letters*, v. 200, p. 331-343.

Breckenridge, R.M., Lewis, R.S., Adema, G.W., and Weisz, D.W., 2003, Miocene and younger faults in Idaho: Idaho Geological Survey, Map 8.

Brown, R.W., Beucher, R., Roper, S., Persano, C., Stuart, F., and Fitzgerald, P., 2013, Natural age dispersion arising from the analysis of broken crystals. Part I: Theoretical basis and implications for the apatite (U-Th)/He thermochronometer: *Geochimica et Cosmochimica Acta*, v. 122, p. 478-497, doi: 10.1016/j.gca.2013.05.041.

Byerly, A., Tikoff, B., Kahn, M., Jicha, B., Gaschnig, R., and Fayon, A.K., 2016, Internal fabrics of the Idaho batholith, USA: *Lithosphere*, doi:10.1130/L551.1.

Byerly, B.L., and Lassiter, J.C., 2012, Evidence from mantle xenoliths for lithosphere removal beneath the central Rio Grande Rift: *Earth and Planetary Science Letters*, v. 355-356, p. 82-93, doi: 10.1016/j.epsl.2012.08.034.

Camp, V.E., 1995, Mid-Miocene propagation of the Yellowstone mantle plume head beneath the Columbia River basalt source region: *Geology*, v. 23, no. 5, p. 435-438, doi: 10.1130/0091-7613(1995)023<0435:MMPOTY>2.3.CO;2.

Camp, V. E., & Ross, M. E., 2004, Mantle dynamics and genesis of mafic magmatism in the intermontane Pacific Northwest: *Journal of Geophysical Research: Solid Earth*, v. 109, no. 8, p. 1–14, doi: 10.1029/2003JB002838.

Camp, V.E., and Hanan, B.B., 2008, A plume-triggered delamination origin for the Columbia River Basalt Group: *Geosphere*, v. 4, no. 3, p. 480-495, doi: 10.1130/GES00175.1.

Canada, A.S., Cassel, E.J., Stockli, D.F., Smith, M.E., Jicha, B.R., and Singer, B.S., 2019, Accelerating exhumation in the Eocene North American Cordilleran hinterland:

Implications from detrital zircon (U-Th)/(He-Pb) double dating: *GSA Bulletin*, v. 132, p. 198-214, doi: 10.1130/B35160.1.

- Casey, M., Ebinger, C., Keir, D., Gloaguen, R., and Mohamed, F., 2006, Strain accommodation in transitional rifts: Extension by magma intrusion and faulting in Ethiopian rift magmatic segments, *in* Yirgu, G., Ebinger, C.J., & Maguire, P.K.H., eds., *The Afar Volcanic Province within the East African Rift System*: Geological Society, London, Special Publications, v. 259, p. 143-163.
- Cassel, E. J., Breecker, D. O., Henry, C. D., Larson, T. E., and Stockli, D. F., 2014, Profile of a paleo-orogen: High topography across the present-day Basin and Range from 40 to 23 Ma: *Geology*, v. 42, no. 11, p. 1007–1010, doi: 10.1130/g35924.1.
- Cassel, E.J., Smith, M.E., and Jicha, B.R., 2018, The impact of slab rollback on Earth's surface: Uplift and extension in the hinterland of the North American Cordillera: *Geophysical Research Letters*, v. 45, p. 10996-11004, doi: 10.1029/2018GL079887.
- Chetel, L.M., Janecke, S.U., Carroll, A.R., Beard, B.L., Johnson, C.M., and Singer, B.S., 2011, Paleogeographic reconstruction of the Eocene Idaho River, North American Cordillera: *Geological Society of America Bulletin*, v. 123, p. 71–88, doi:10.1130/B30213.1.
- Christiansen, R.L., 2001, The Quaternary and Pliocene Yellowstone Plateau volcanic field of Wyoming, Idaho, and Montana: U.S. Geological Survey Professional Paper 729-G, 120 p.
- Clemens, D.M., 1993, Tectonics and silicic volcanic stratigraphy of the western Snake River Plain, southwestern Idaho [MS thesis]: Arizona State University, 209 p.
- Clemens, D.M., and Wood, S.H., 1993, Late Cenozoic volcanic stratigraphy and geochronology of the Mount Bennett Hills, central Snake River Plain, Idaho: *Isochron/West*, v. 60, p. 3-14.
- Curry, M.A.E., Barnes, J.B., and Colgan, J.P., 2016, Testing fault growth models with low-temperature thermochronology in the northwest Basin and Range, USA: *Tectonics*, v. 35, p. 2467-2492, doi: 10.1002/2016TC004211.
- DeCelles, P. G., 2004, Late Jurassic to Eocene evolution of the Cordilleran thrust belt and foreland basin system, western U.S.A.: *American Journal of Science*, v. 304, no. 2, p. 105–168, doi: 10.2475/ajs.304.2.105.
- DeCelles, P., Ducea, M.N., Kapp, P., and Zandt, G., 2009, Cyclicality in Cordilleran orogenic systems: *Nature Geoscience*, v. 2, p. 251-257, doi: 10.1038/ngeo469.

- Densmore, A.L., Dawers, N.H., Gupta, S., Guidon, R., and Goldin, T., 2004, Footwall topographic development during continental extension: *Journal of Geophysical Research*, v. 109, F03001, doi: 10.1029/2003JF000115.
- Dickinson, W.R., 2004, Evolution of the North American Cordillera: *Annual Reviews in Earth and Planetary Science*, v. 32, p. 13-45, doi: 10.1146/annurev.earth.32.101802.120257.
- Ducea, M.N., 2001, The California arc: Thick granitic batholiths, eclogitic residues, lithospheric-scale thrusting, and magmatic flare-ups: *GSA Today*, v. 11, no. 11, p. 4–10, doi:10.1130/1052-5173(2001)011<0004:TCATGB>2.0.CO;2.
- Dumitru, T.A., Ernst, W.G., Wright, J.E., Wooden, J.L., Wells, R.E., Farmer, L.P., Kent, A.J.R., and Graham, S.A., 2013, Eocene extension in Idaho generated massive sediment floods into the Franciscan trench and into the Tye, Great Valley, and Green River basins: *Geology*, v. 41, no. 2, p. 187-190, doi: 10.1130/G33746.1.
- Eaton, G.P., 1982, The Basin and Range Province: Origin and tectonic significance: *Annual Review of Earth and Planetary Sciences*, v. 10, p. 409, doi: 10.1146/annurev.earth.10.050182.002205.
- Ekren, E.B., McIntyre, D.H., Bennett, E.H., and Malde, H.E., 1981, Geologic map of Owyhee County, Idaho, west of longitude 116°W: U.S. Geological Survey Miscellaneous Investigations Map I-1256, scale 1:24,000.
- Ellis, M.A., and Barnes, J.B., 2015, A global perspective on the topographic response to fault growth: *Geosphere*, v. 11, p. 1008-1023, doi: 10.1130/GES01156.1.
- English, J.M., and Johnston, S.T., 2004, The Laramide orogeny: What were the driving forces?: *International Geology Review*, v. 46, p. 833-838, doi: 10.2747/0020-6814.46.9.833.
- Farley, K.A., 2000, Helium diffusion from apatite: General behavior as illustrated by Durango fluorapatite: *Journal of Geophysical Research*, v. 105, no. B2, p. 2903-2914.
- Fayon, A.K., Tikoff, B., Kahn, M., and Gaschnig, R.M., 2017, Cooling and exhumation of the southern Idaho batholith: *Lithosphere*, v. 9, no. 2, p. 299-314, doi: 10.1130/L565.1.
- Flowers, R.M., Ketcham, R.A., Shuster, D.L., and Farley, K.A., 2009, Apatite (U-Th)/He thermochronometry using a radiation damage accumulation and annealing model: *Geochimica et Cosmochimica Acta*, v. 73, p. 2347-2365, doi: 10.1016/j.gca.2009.01.015.
- Flowers, R.M., Shuster, D.L., Wernicke, B.P., and Farley, K.A., 2007, Radiation damage control on apatite (U-Th)/He dates from the Grand Canyon region, Colorado Plateau: *Geology*, v. 35, no. 5, p. 447-450, doi: 10.1130/G2347A.1.

- Forester, C.S., and Wood, S. H., 2012, Geologic map of the Holland Gulch quadrangle, Payette and Washington counties, Idaho: Idaho Geological Survey Technical Report 12-1, scale 1:24,000, 1 sheet.
- Foster, D.A., and Raza, A., 2002, Low-temperature thermochronological record of exhumation of the Bitterroot metamorphic core complex, northern Cordilleran orogen: *Tectonophysics*, v. 349, p. 23-36, doi: 10.1016/S0040-1951(02)00044-6.
- Foster, D.A., Grice, W., and Kalakay, T., 2010, Extension of the Anaconda metamorphic core complex:  $^{40}\text{Ar}/^{39}\text{Ar}$  thermochronology and implications for Eocene tectonics of the northern Rocky Mountains and the Boulder batholith: *Lithosphere*, v. 2, no. 4, p. 232-246, doi: 10.1130/L94.1.
- Gaschnig, R.M., Vervoort, J.D., Lewis, R.S., and McClelland, W.C., 2010, Migrating magmatism in the northern US Cordillera: In situ U-Pb geochronology of the Idaho batholith: *Contributions to Mineralogy and Petrology*, v. 159, p. 863–883, doi:10.1007/s00410-009-0459-5.
- Gaschnig, R.M., Vervoort, J.D., Lewis, R.S., and Tikoff, B., 2011, Isotopic evolution of the Idaho Batholith and Challis Intrusive Province, Northern US Cordillera: *Journal of Petrology*, v. 52, no. 12, p. 2397-2429, doi: 10.1093/petrology/egr050.
- Gautheron, C., Tassan-Got, L., Barabrand, J., and Pagel, M., 2009, Effect of alpha-damage annealing on apatite (U-Th)/He thermochronology: *Chemical Geology*, v. 266, p. 157-170, doi: 10.1016/j.chemgeo.2009.06.001.
- Gehrels, G., Rusmore, M., Woodsworth, G., Crawford, M., Andronicos, C., Hollister, L., Patchett, J., Ducea, M., Butler, R., Klepeis, K., Davidson, C., Friedman, R., Haggart, J., Mahoney, B., Crawford, W., Pearson, D., and Girardi, J., 2009, U-Th-Pb geochronology of the Coast Mountains batholith in north-coastal British Columbia: Constraints on age and tectonic evolution: *Geological Society of America Bulletin*, v. 121, p. 1341–1361, doi:10.1130/B26404.1.
- Geist, D., and Richards, M., 1993, Origin of the Columbia Plateau and Snake River plain: Deflection of the Yellowstone plume: *Geology*, v. 21, p. 789-792, doi: 10.1130/0091-7613(1993)021<0789:OOTCPA>2.3.CO;2.
- Giorgis, S., McClelland, W., Fayon, A., Singer, B.S., and Tikoff, B., 2008, Timing of deformation and exhumation in the western Idaho shear zone, McCall, Idaho: *GSA Bulletin*, v. 120, p. 1119-1133, doi: 10.1130/B26291.1.
- Glen, J. M. G., and Ponce, D. A., 2002, Large-scale fractures related to inception of the Yellowstone hotspot: *Geology*, v. 30, no. 7, p. 647–650, doi: 10.1130/0091-7613(2002)030<0647:LSFRTI>2.0.CO;2.

- Hales, T.C., Abt, D.L., Humphreys, E.D., and Roering, J.J., 2005, A lithospheric instability origin for Columbia River flood basalts and Wallowa Mountains uplift in northeast Oregon: *Nature*, v. 438, p. 842-845, doi: 10.1038/nature04313.
- Heller, P.L., and Liu, L., 2016, Dynamic topography and vertical motion of the U.S. Rocky Mountain region prior to and during the Laramide orogeny: *GSA Bulletin*, v. 128, p. 973-988, doi: 10.1130/B31431.1.
- Heller, P.L., Peterman, Z.E., O'Neil, J.R., and Shafi-qullah, M., 1985, Isotopic provenance of sandstones from the Eocene Tyee Formation, Oregon Coast Range: *Geological Society of America Bulletin*, v. 96, p. 770-780, doi:10.1130/0016-7606(1985)96<770:IPOSF>2.0.CO;2.
- Hildebrand, R.S., and Whalen, J.B., 2014, Arc and slab-failure magmatism in Cordilleran batholiths II – The Cretaceous Peninsular Ranges batholith of southern and Baja California: *Geoscience Canada*, v. 41, p. 399-458, doi: 10.12789/geocanj.2014.41.059.
- Hill, D.P., and Pakiser, L.C., 1967, Seismic-refraction study of crustal structure between the Nevada Test Site and Boise, Idaho: *Geological Society of America Bulletin*, v. 78, no. 6, p. 685-704.
- Hiza, M.M., 1999, The geochemistry and geochronology of the Eocene Absaroka volcanic province northern Wyoming and southwest Montana, USA [Ph.D. dissertation]: Oregon State University, 261 p.
- Hooper, P.R., Camp, V.E., Reidel, S.P., and Ross, M.E., 2007, The origin of the Columbia River flood basalt province: Plume versus nonplume models, *in* Foulger, G.R., and Jurdy, D.M., eds., *Plates, plumes, and planetary processes*: Geological Society of America Special Paper 430, p. 635-668, doi: 10.1130/2007.2430(30).
- Humphreys, E.D., 1995, Post-Laramide removal of the Farallon slab, western United States: *Geology*, v. 23, no. 11, p. 987-990, doi: 10.1130/0091-7613(1995)023<0987:PLROTF>2.3.CO;2.
- Janecke, S.U., 1994, Sedimentation and paleogeography of an Eocene to Oligocene rift zone, Idaho and Montana: *GSA Bulletin*, v. 106, p. 1083-1095.
- Johnson, K.M., Lewis, R.S., Bennett, E.H., and Kiilsgaard, T.H., 1988, Cretaceous and Tertiary intrusive rocks of south-central Idaho, *in* Link, P.K., and Hackett, W.R., eds., *Guidebook to the Geology of Central and Southern Idaho*: Idaho Geological Survey Bulletin 27, p. 55-86.
- Karlstrom, L., Murray, K.E., and Reiners, P.W., 2019, Bayesian Markov-Chain Monte Carlo inversion of low-temperature thermochronology around two 8-10 m wide Columbia River Flood basalt dikes: *Frontiers in Earth Science*, v. 7, doi: 10.3389/feart.2019.00090.

- Kasbohm, J., and Schoene, B., 2018, Rapid eruption of the Columbia River flood basalt and correlation with the mid-Miocene climate optimum: *Science Advances*, v. 4, no. 9, doi: 10.1126/sciadv.aat8223.
- Kent-Corson, M.L., Sherman, L.S., Mulch, A., and Chamberlain, C.P., 2006, Cenozoic topographic and climatic response to changing tectonic boundary conditions in Western North America: *Earth and Planetary Science Letters*, v. 252, p. 453-466, doi: 10.1016/j.epsl.2006.09.049.
- Kessler, J.A., Bradbury, K.K., Evans, J.P., Pulsipher, M.A., Schmitt, D.R., Shervais, J.W., Rowe, F.E., and Varriale, J., 2017, Geology and in situ stress of the MH-2 borehole, Idaho, USA: Insights into western Snake River Plain structure from geothermal exploration drilling: *Lithosphere*, v. 9, p. 476-498, doi: 10.1130/L609.1.
- Ketcham, R.A., 2005, Forward and inverse modeling of low-temperature thermochronometry data: *Reviews in Mineralogy and Geochemistry*, v. 58, p. 275-314, doi: 10.2138/rmg.2005.58.11.
- Ketcham, R.A., Gautheron, C., and Tassan-Got, L., 2011, Accounting for long alpha-particle stopping distances in (U-Th-Sm)/He geochronology: Refinement of the baseline case: *Geochimica et Cosmochimica Acta*, v. 75, p. 7779-7791, doi: 10.1016/j.gca.2011.10.011.
- Kiilsgaard, T.H., and Lewis, R.S., 1983, Chapter B: Plutonic rocks of Cretaceous age and faults in the Atlanta lobe of the Idaho batholith, Challis quadrangle, *in* McIntyre, D.H., ed., *Symposium on the Geology and Mineral Deposits of the Challis 1°x2° Quadrangle, Idaho*: U.S. Geological Survey Bulletin 1658 A-S.
- Kimmel, P. G., 1982, Age and tectonic setting of the lacustrine sediments of the western Snake River Plain, Oregon and Idaho: *Idaho Bureau of Mines and Geology Bulletin*, v. 26, p. 559-578.
- Korenaga, T., and Korenaga, J., 2008, Subsidence of normal oceanic lithosphere, apparent thermal expansivity, and seafloor flattening: *Earth and Planetary Science Letters*, v. 268, p. 41-51, doi: 10.1016/j.epsl.2007.12.022.
- Lackey, J.S., Valley, J.W., Chen, J.H., and Stockli, D.F., 2008, Dynamic magma systems, crustal recycling, and alteration in the central Sierra Nevada batholith: The oxygen isotope record: *Journal of Petrology*, v. 49, p. 1397-1426, doi: 10.1093/petrology/egn030.
- Larimer, J.E., Yanites, B.J., Philips, W., and Mittelstaedt, E., 2018, Late Miocene rejuvenation of central Idaho landscape evolution: A case for surface processes driven by plume-lithosphere interaction: *Lithosphere*, v. 11, p. 59-72, doi: 10.1130/L476.1.
- Leopold, E.B. and Denton, M.F., 1987, Comparative age of grassland and steppe east and west of the northern rocky mountain: *Annals of the Missouri Botanical Garden*, p. 841-867.

- Lewis, R.S., Link, P.K., Standford, L.R., and Long, S.P., 2012, Geologic map of Idaho: Idaho Geologic Survey, scale 1:750,000.
- Lielke, K., Manchester, S.R., and Meyer, H.W., 2012, Reconstructing the environment of the northern Rocky Mountains during the Eocene/Oligocene transition: Constraints from the palaeobotany and geology of southwestern Montana, USA: *Acta Palaeobotanica*, v. 52, p. 317-358.
- Lindgren, W., 1904, A geological reconnaissance across the Bitterroot Range and Clearwater Mountains in Montana and Idaho: U.S. Geological Survey Professional Paper 27, 122 p.
- Liu, L., and Stegman, D.R., 2012, Origin of Columbia River flood basalt controlled by propagating rupture of the Farallon slab: *Nature*, v. 482, p. 386-389, doi: 10.1038/nature10749.
- Liu, S., and Currie, C.A., 2015, Farallon plate dynamics prior to the Laramide orogeny: Numerical models of flat subduction: *Tectonophysics*, v. 666, p. 33-47, doi: 10.1016/j.tecto.2015.10.010.
- Long, S. P., 2012, Magnitudes and spatial patterns of erosional exhumation in the Sevier hinterland, eastern Nevada and western Utah, USA: Insights from a Paleogene paleogeographic map: *Geosphere*, v. 8, no. 4, p. 881–901, doi: 10.1130/GES00783.1.
- Love, R.L., Lewis, R.S., Wood, S.H., and Feeney, D.M., 2020, U-Pb ages, mapping, and biostratigraphy of the Payette Formation and Idaho Group north of the western Snake River Plain: Implications for hydrocarbon exploration: *AAPG Bulletin* (in press).
- Mabey, D.R., 1976, Interpretation of a gravity profile across the western Snake River Plain, Idaho: *Geology*, v. 4, no. 1, p. 53–55.
- Malde, H. E., 1959, Fault Zone along Northern Boundary of Western Snake River Plain, Idaho: *Science*, v. 130, no. 3370, p. 272–272, doi: 10.1126/science.130.3370.272.
- Malde, H. E., 1991, Quaternary geology and structural history of the Snake River Plain, Idaho and Oregon: *The Geology of North America*, v. 2, p. 251–281.
- Min, G., and Hou, G., 2019, Mechanism of the Mesozoic African rift system: Paleostress field modeling: *Journal of Geodynamics*, v. 132, doi: 10.1016/j.jog.2019.101655.
- Mitchell, N.A., and Yanites, B.J., 2019, Spatially variable increase in rock uplift in the northern U.S. Cordillera recorded in the distribution of river knickpoints and incision depths: *Journal of Geophysical Research: Earth Surface*, v. 124, doi: 10.1029/2018JF004880.

- Montgomery, D.R., and Brandon, M.T., 2002, Topographic controls on erosion rates in tectonically active mountain ranges: *Earth and Planetary Science Letters*, v. 201, p. 481-489, doi: 10.1016/S0012-821X(02)00725-2.
- Morgan, W. J., 1972, Deep mantle convection plumes and plate motions: *AAPG Bulletin*, v. 56, no. 2, p. 203–213.
- Murray, K.E., Orme, D.A., and Reiners, P.W., 2014, Effects of U-Th-rich grain boundary phases on apatite helium ages: *Chemical Geology*, v. 390, p. 135-151, doi: 10.1016/j.chemgeo.2014.09.023.
- Murray, K.E., Braun, J., and Reiners, P.W., 2018, Toward robust interpretation of low-temperature thermochronometers in magmatic terranes: *Geochemistry, Geophysics, Geosystems*, v. 19, p. 3739-3763, doi: 10.1029/2018GC007595.
- Nelson, R. A., Patton, T. L., & Morley, C. K., 1992, Rift-segment interaction and its relation to hydrocarbon exploration in continental rift systems: *American Association of Petroleum Geologists Bulletin*, v. 76, p. 1153–1160.
- Othberg, K.L., and Stanford, L.R., 1992, Geologic map of the Boise Valley and adjoining areas, western Snake River Plain, Idaho: Idaho Geological Survey Geologic Map Series, scale 1:100,000.
- Pansze, A.J., Jr., 1975, Geology and ore deposits of the Silver City – De Lamar – Flint region, Owyhee County, Idaho: Idaho Bureau of Mines and Geology Pamphlet 161, 91 p.
- Parsons, B., and Sclater, J.G., 1977, An analysis of the variation of ocean floor bathymetry and heat flow with age: *Journal of Geophysical Research*, v. 82, p. 803-827.
- Payne, S.J., McCaffrey, R., King, R.W., and Kattenhorn, S.A., 2012, A new interpretation of deformation rates in the Snake River Plain and adjacent basin and range regions based on GPS measurements: *Geophysical Journal International*, v. 189, p. 101-122, doi: 10.1111/j.1365-246X.2012.05370.x.
- Peace, A.L., Phethean, J.J.J., Franke, D., Foulger, G.R., and others, 2019, A review of Pangaea dispersal and large igneous provinces – In search of a causative mechanism: *Earth Science Reviews*, in press.
- Pe-Piper, G., Jansa, L.F., and Lambert, R. St. J., 1992, Early Mesozoic magmatism on the eastern Canadian margin: Petrogenetic and tectonic significance, *in* Puffer, J.H., and Ragland, P.C., eds., *Eastern North American Mesozoic Magmatism: Geological Society of America Special Paper 268*, doi: 10.1130/SPE268-p13.
- Philpotts, A.R., 1992, A model for emplacement of magma in the Mesozoic Hartford basin, *in* Puffer, J.H., and Ragland, P.C., eds., *Eastern North American Mesozoic Magmatism: Geological Society of America Special Paper 268*, doi: 10.1130/SPE268-p137.

- Pierce, K.L., and Morgan, L.A., 1992, The track of the Yellowstone hot spot: Volcanism, faulting, and uplift, *in* Link, P.K., Kuntz, M.A., and Platt, L.B., eds., *Regional Geology of Eastern Idaho and Western Wyoming: Geological Society of America Memoir 179*.
- Premo, W.R., Morton, D.M., Wooden, J.L., and Fanning, C.M., 2014, U-Pb zircon geochronology of plutonism in the northern Peninsular Ranges batholith, southern California: Implications for the Late Cretaceous tectonic evolution of southern California, *in* Morton, D.M., and Miller, F.K., eds., *Peninsular Ranges Batholith, Baja California and Southern California: Geological Society of America Memoir 211*, p. 145–180, doi:10.1130/2014.1211(04).
- Reidel, S.P., Camp, V.E., Tolan, T.L., and Martin, B.S., 2013, The Columbia River flood basalt province: Stratigraphy, areal extent, volume and physical volcanology, *in* Reidel, S.P., Camp, V.E., Ross, M.E., Wolff, J.A., Martin, B.S., Tolan, T.L., and Wells, R.E., eds., *The Columbia River Basalt Province: Geological Society of America Special Paper v. 497*, p. 1-43.
- Reiners, P. W., and Farley, K. A., 2001, Influence of crystal size on apatite (U-Th)/He thermochronology: An example from the Bighorn Mountains, Wyoming: *Earth and Planetary Science Letters*, v. 188, p. 413– 420.
- Reiners, P.W., and Brandon, M., 2006, Using thermochronology to understand orogenic erosion: *Annual Review of Earth and Planetary Sciences*, v. 34, no. 1, p. 419-466, doi: 10.1146/annurev.earth.34.031405.125202.
- Ricketts, J.W., Kelley, S.A., Karlstrom, K.E., Schmandt, B., Donahue, M.S., and van Wijk, J., 2016, Synchronous opening of the Rio Grande rift along its entire length at 25-10 Ma supported by apatite (U-Th)/He and fission-track thermochronology, and evaluation of possible driving mechanisms: *GSA Bulletin*, v. 128, p. 397-424, doi: 10.1130/B31223.1.
- Saleeby, J.B., Ducea, M.N., Busby, C.J., Nadin, E.S., and Whetmore, P.H., 2008, Chronology of pluton emplacement and regional deformation in the southern Sierra Nevada batholith, California, *in* Wright, J.E., and Shervais, J.W., eds., *Ophiolites, Arcs, and Batholiths: A Tribute to Cliff Hopson: Geological Society of America Special Paper 438*, p. 397-427, doi: 10.1130/2008.2438(14).
- Schwartz, T.M., Methner, K., Mulch, A., Graham, S.A., and Chamberlain, C.P., 2019, Paleogene topographic and climatic evolution of the Northern Rocky Mountains from integrated sedimentary and isotopic data: *GSA Bulletin*, v. 131, p. 1203-1223, doi: 10.1130/B32068.1.
- Shervais, J.W., Shroff, G., Vetter, S.K., Matthews, S., Hanan, B.B., and McGee, J.J., 2002, Origin and evolution of the western Snake River Plain: Implications from stratigraphy, faulting, and the geochemistry of basalts near Mountain Home, Idaho, *in* Bonnicksen, B.,

- White, C.M., and McCurry, M., eds., Tectonic and Magmatic Evolution of the Snake River Plain Volcanic Province: Idaho Geological Survey Bulletin 30, p. 343-361.
- Shervais, J.W., and Hanan, B.B., 2008, Lithospheric topography, tilted plumes, and the track of the Snake River-Yellowstone hot spot: *Tectonics*, v. 27, TC5004, doi: 10.1029/2007TC002191.
- Shervais, J.W., Evans, J.P., Christiansen, E.J., Schmitt, D.R., Liberty, L.M., Blackwell D.D., and others, 2011, Hotspot: The Snake River geothermal drilling project – An overview: *GRC Transactions*, v. 35, p. 995-1003.
- Shuster, D.L., Flowers, R.M., and Farley, K.A., 2006, The influence of natural radiation damage on helium diffusion kinetics in apatite: *Earth and Planetary Science Letters*, v. 249, p. 148-161, doi:10.1016/j.epsl.2006.07.028.
- Smith, G. R., Swirydczuk, K., Kimmel, P. G., & Wilkinson, B. H., 1982, Fish biostratigraphy of late Miocene to Pleistocene sediments of the western Snake River Plain, Idaho: *Cenozoic Geology of Idaho: Idaho Bureau of Mines and Geology Bulletin*, v. 26, p. 519–541.
- Smith, R. B., and Braile, L. W., 1994, The yellowstone hotspot: *Journal of Volcanology and Geothermal Research*, v. 61, no. 3–4, p. 121–187.
- Smith, R.B., and Siegel, L.J., 2000, *Windows into the Earth – The Geologic Story of Yellowstone and Grand Teton National Parks*: Oxford University Press, 256 p.
- Snell, K., Thompson, J.M., Foreman, B., Wernicke, B., Chamberlain, C.P., Eiler, J.M., and Koch, P.L., 2011, Paleoclimate and paleoelevation in the western US Cordillera, 80 Ma to Present: American Geophysical Union, December 2011, abstract id. T22C-05.
- Spiegel, C., Kohn, B., Belton, D., Berner, Z., and Gleadow, A., 2009, Apatite (U-Th-Sm)/He thermochronology of rapidly cooled samples: The effect of He implantation: *Earth and Planetary Science Letters*, v. 285, p. 105-114, doi: 10.1016/j.epsl.2009.05.045.
- Stevens, L.M., Bendick, R., and Baldwin, J.A., 2017, Synconvergent exhumation of metamorphic core complexes in the northern North American Cordillera: *Geology*, v. 45, no. 6, p. 495-498, doi: 10.1130/G38802.1.
- Stockli, D.F., Farley, K.A., and Dumitru, T.A., 2000, Calibration of the apatite (U-Th)/He thermochronometer on an exhumed fault block, White Mountains, California: *Geology*, v. 28, no. 11, p. 983-986.
- Stockli, D., 2005, Application of low temperature thermochronometry to extensional tectonic settings: *Reviews in Mineralogy and Geochemistry*, v. 58, p. 411-448.

- Sun, J., and Zhang, Z., 2008, Palynological evidence for the Mid-Miocene Climatic Optimum recorded in Cenozoic sediments of the Tian Shan Range, northwestern China: *Global and Planetary Change*, v. 64, p. 53-68, doi: 10.1016/j.gloplacha.2008.09.001.
- Sweetkind, D.S., and Blackwell, D.D., 1989, Fission-track evidence of the Cenozoic thermal history of the Idaho batholith: *Tectonophysics*, v. 157, p. 241-250.
- Swirydczuk, K., Wilkinson, B. H., & Smith, G. R., 1979, The Pliocene Glens Ferry oolite: Lake-margin carbonate deposition in the southwestern Snake River plain: *Journal of Sedimentary Research*, v. 49, no. 3, p. 995–1004.
- Turcotte, D.L., and Schubert, G., 1982, *Geodynamics: Applications of continuum physics to geological problems*: John Wiley and Sons, New York.
- Umpleby, J.B., 1912, An old erosion surface in Idaho: Its age and value as a datum plane: *The Journal of Geology*, v. 20, p. 139-147, doi: 10.1086/621941.
- Vermeesch, P., Seward, D., Latkoczy, C., Wipf, M., Gunther, D., and Baur, H., 2007, Alpha-emitting mineral inclusions in apatite, their effect on (U-Th)/He ages, and how to reduce it: *Geochimica et Cosmochimica Acta*, v. 71, no. 7, p. 1737-1746, doi: 10.1016/j.gca.2006.09.020.
- Vogl, J.J., Foster, D.A., Fanning, C.M., Kent, K.A., Rodgers, D.W., and Diedesch, T., 2012, Timing of extension in the Pioneer metamorphic core complex with implications for the spatial-temporal pattern of Cenozoic extension and exhumation in the northern U.S. Cordillera: *Tectonics*, v. 31, TC1008, doi: 10.1029/2011TC002981.
- Vogl, J.J., Min, K., Carmenate, A., Foster, D.A., and Marsellos, A., 2014, Miocene regional hotspot-related uplift, exhumation, and extension north of the Snake River Plain: Evidence from apatite (U-Th)/He thermochronology: *Lithosphere*, v. 6, no. 2, p. 108-123, doi: 10.1130/L208.1.
- Wegmann, K.W., Zurek, B.D., Regalla, C.A., and others, 2007, Position of the Snake River watershed divide as an indicator of geodynamic processes in the greater Yellowstone region, western North America: *Geosphere*, v. 3, no. 4, p. 272-281, doi: 10.1130/GES00083.1.
- Wells, M.L., Snee, L.W., and Blythe, A.E., 2000, Dating of major normal fault systems using thermochronology: An example from the Raft River detachment, Basin and Range, western United States: *Journal of Geophysical Research*, v. 105, p. 16,303–16,327, doi:10.1029 /2000JB900094.
- Wobus, C., Whipple, K.X., Kirby, E., Snyder, N., Johnson, J., Spyropolou, K., Crosby, B., and Sheehan, D., 2006, Tectonics from topography: Procedures, promise, and pitfalls, *in* Willett, S.D., Hovius, N., Brandon, M.T., and Fisher, D., eds., *Tectonics, Climate, and*

Landscape Evolution: Geological Society of America Special Paper 398, p. 55w-74, doi: 10.1130/2006.2398(04).

- Wolfe, J.A., Forest, C.E., and Molnar, P., 1998, Paleobotanical evidence of Eocene and Oligocene paleoaltitudes in midlatitude western North America: *GSA Bulletin*, v. 110, no. 5, p. 664-678, doi: 10.1130/0016-7606(1998)110<0664:PEOEAO>2.3.CO;2.
- Wood, S.H., and Anderson, J.E., 1981, Chapter 2-Geology, *in* Mitchell, J.C., ed., Geological, hydrological, geochemical and geophysical investigations of the Nampa-Caldwell and adjacent areas, southwestern Idaho: Idaho Department of Water Resources Water Information Bulletin No. 30, Geothermal Investigations in Idaho, Part 11, p. 9-31.
- Wood, S.H., and Clemens, D.M., 2002, Geologic and tectonic history of the western Snake River Plain, Idaho and Oregon, *in* B. Bonnicksen, C.M. White, and M. McCurry, eds., Tectonic and Magmatic Evolution of the Snake River Plain Volcanic Province: Idaho Geological Survey Bulletin 30, p. 69-103.
- Woodburne, M.O., Gunnell, G.F., and Stucky, R.K., 2009, Climate directly influence Eocene mammal faunal dynamics in North America: *Proceedings of the National Academy of Sciences of the United States of America*, v. 106, p. 13399-13403, doi: 10.1073/pnas.0906802106..
- Yonkee, W.A., and Weil, A.B., 2015, Tectonic evolution of the Sevier and Laramide belts within the North American Cordillera orogenic system: *Earth-Science Reviews*, v. 150, p. 531-593, doi: 10.1016/j.earscirev.2015.08.001.
- Zachos, J., Pagani, M., Sloan, L., Thomas, E. and Billups, K., 2001, Trends, rhythms, and aberrations in global climate 65 Ma to present: *Science*, v. 292, no. 5517, p. 686-693.
- Zachos, J.C., Dickens, G.R., and Zeebe, R.E., 2008, An early Cenozoic perspective on greenhouse warming and carbon-cycle dynamics: *Nature*, v. 451, p 279-283, doi: 10.1038/nature06588.
- Zhou, Q., and Liu, L., 2019, Topographic evolution of the western United States since the early Miocene: *Earth and Planetary Science Letters*, v. 514, p. 1-12, doi: 10.1016/j.epsl.2019.02.029.
- Ziegler, P.A., and Cloetingh, S., 2004, Dynamic processes controlling evolution of rifted basins: *Earth-Science Review*, v. 64, p. 1-50, doi: 10.1016/S0012-8252(03)00041-2.